

ZERO FIELD LEVEL CROSSING IN
MOLECULAR HYDROGEN

by

JACOB VAN DER LINDE

B.Sc., University of British Columbia, 1967

A THESIS SUBMITTED IN PARTIAL FULFILLMENT OF
THE REQUIREMENTS FOR THE DEGREE OF
DOCTOR OF PHILOSOPHY

in the Department
of
PHYSICS

We accept this thesis as conforming to the
required standard

THE UNIVERSITY OF BRITISH COLUMBIA

September, 1970

In presenting this thesis in partial fulfilment of the requirements for an advanced degree at the University of British Columbia, I agree that the Library shall make it freely available for reference and study. I further agree that permission for extensive copying of this thesis for scholarly purposes may be granted by the Head of my Department or by his representatives. It is understood that copying or publication of this thesis for financial gain shall not be allowed without my written permission.

Department of Physics

The University of British Columbia
Vancouver 8, Canada

Date Sept 29, 1970

ABSTRACT

The lifetimes of the $3d^1\Sigma(v=0)$ $J=1$, 2 and 3 states have been measured using zero-field level crossing techniques. The transitions observed were the R-branch members of the $3d^1\Sigma \rightarrow 2p^1\Sigma$ transition. The upper state is excited in a discharge between two capacitor plates to which a radio-frequency voltage is applied. The measurements were made using first a 180 MHz R.F. source and later using a 450 MHz source. Polarization of emitted light was measured by rotating a polaroid in the beam and phase sensitive detecting the resulting modulation.

The depolarization curves obtained by plotting the magnetic field strength against the polarization of the $R(0)$, $R(1)$, $R(2)$ lines yield halfwidths, when extrapolated to zero pressure, of $2.37 \pm .12$ gauss, $2.60 \pm .15$ gauss and $3.25 \pm .25$ gauss. The halfwidths vary linearly with pressure in the discharge cell yielding collision cross-sections of roughly 1.5×10^{-14} cm 2 .

Using the high field Landé g values of these states, their lifetimes are $(2.66 \pm .12) \times 10^{-8}$ sec., $(3.83 \pm .2) \times 10^{-8}$ sec., and $(3.93 \pm .25) \times 10^{-8}$ sec. for $J=1$, 2 and 3 respectively. The discrepancy between the first and the latter two lifetimes is discussed.

TABLE OF CONTENTS

CHAPTER	PAGE
I INTRODUCTION	1
II THEORY	8
§2.1 Introduction	8
§2.2 The Magnetic Field Dependence of Polarization in Classical Terms	8
§2.3 Quantum-Mechanical Description of Level Crossing	14
§2.4 The $3d^1\Sigma$ Levels of H_2	18
§2.5 The Excitation Matrix Elements Q	22
III EXPERIMENTAL DETAILS	28
§3.1 Experimental Arrangement	28
§3.2 The Discharge	30
§3.3 The Optical System	34
§3.4 The Vacuum System	37
§3.5 R.F. Supplies and Coupling	40
§3.6 Helmholtz Coils	42
§3.7 Current Supplies for Helmholtz Coils	46
§3.8 Lock-in Amplifier	49
§3.9 Rotating Polaroid	50
§3.10 The Variable Quarter-Wave Plate . .	50
§3.11 Photomultiplier	54
§3.12 X-Y Recorder	54
§3.13 Liquid Nitrogen Bath	55
§3.14 Data Processing	56

CHAPTER	PAGE
IV EXPERIMENTAL RESULTS	57
§4.1 Lifetimes	57
§4.2 Collision Cross-sections	64
§4.3 Polarization	68
§4.4 Upper State Populations	69
§4.5 Experimental Errors	71
a) Discharge Stability	71
b) Magnetic Field	72
c) Pressure in the Discharge .	73
d) Temperature in the Discharge	73
e) Cascading	74
f) Coherence Narrowing	74
g) R.F. Broadening	75
§4.6 Helium 4^1D Lifetime Compared With That Obtained From Other Experiments	76
V DISCUSSION OF RESULTS AND CONCLUSION . . .	80
§5.1 Introduction	80
§5.2 Hyperfine Effects	80
§5.3 Electronic Wave Function Variation with J	85
§5.4 Conclusion and Suggestions for Further Work	86
APPENDIX I THE TRANSITION MATRIX ELEMENTS . . .	87
APPENDIX II THE $3d^1$ STATES OF H_2	91
§A2.1 Energy Levels and Eigenstates . .	91
§A2.2 The Zeeman Effect	97

	PAGE
APPENDIX III OTHER STATES	102
§A3.1 The $3d^1\Pi^-(v=0)$ J=2 State	102
§A3.2 The 3^1K State	104
REFERENCES AND FOOTNOTES	105

LIST OF TABLES

TABLE	PAGE
I Relative Populations of the First Few Rotational Levels of Hydrogen at Thermal Equilibrium	21
II Properties of Electron Motion in an R.F. Electric and D.C. Magnetic Field	34
III Level Crossing Curve Halfwidths ($3d^1\Pi$ and 3^1K)	103
IV Extrapolated Halfwidths and Lifetimes	64
V Polarization Curves' Halfwidths	65
VI Collision Cross-sections	68
VII Experimental Upper State Populations	70
VIII Lifetime of the 4^1D State of Helium	77
IX Energies of the $3d^1$ Complex of H_2	94
X Expansion Coefficients for the $3d^{1+}$ States	95
XI Relative Intensities of P and R Transitions in the $3d^1\Sigma \rightarrow 2p^1\Sigma (0,0)$ Band	97
XII g-values of the $3d^1\Sigma$ State	99

ILLUSTRATIONS AND FIGURES

FIGURE	PAGE
1 The Singlet States of Hydrogen (H_2)	3
2 The Transitions Observed	4
3 Hanle Effect Co-ordinate System	9
4 Polarization for $\phi=0$	11
5 Polarization for $\phi=\pi/4$	11
6 "Three" Level System	14
7 The Scattering Angle	26
8 The Apparatus	29
9 Cross-Section of Discharge Cell and Capacitor Plates	31
10 The Vacuum System	39
11 180 MHz R.F. Oscillator	41
12 T-Matched Resonant Circuit	43
13 Helmholtz Coil Power Supply	45
14 D.C. Power Amplifier	47
15 -10V to +10V Voltage Sweep Mechanism	48
16 Polaroid Rotator	51
17 Quarter-Wave Plate	53
18 Photomultiplier Wiring Schematic	54
19 Experimental Level-Crossing Curve for the R(0) Line Using 450 MHz Excitation	58
20 Least Squares Fitted Curve for the R(0) Line Using 450 MHz Excitation	59

FIGURE	PAGE
21 Experimental Level-Crossing Curve for the R(0) Line Using 180 MHz Excitation	60
22 Least Squares Fitted Curve for the R(o) Line Using 180 MHz Excitation	61
23 Level Crossing Curve Halfwidth as a Function of Pressure	62
24 Level Crossing Curve Halfwidth as a Function of Pressure	63
25 Experimental Level-Crossing Curve for the Helium $4^1D \rightarrow 2^1P$ Transition	78
26 4^1D Curve Halfwidth as a Function of Pressure	79
27 Zeeman Effect in the Presence of Small Hyperfine Splitting	84
28 The First Few Lines of the R Branch of the $3d^1\Sigma \rightarrow 2p^1\Sigma(0,0)$ band of H ₂	101

ACKNOWLEDGEMENTS

I wish to express my gratitude to Professor F.W. Dalby for suggesting the problem. His supervision of the research, advice and encouragement were invaluable.

I also wish to thank my wife for her help in the preparation of this thesis. Other contributions, both tangible and intangible, have been made by my fellow graduate students.

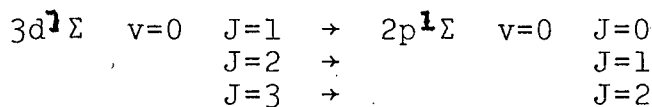
This work was supported by the National Research Council of Canada.

CHAPTER I

INTRODUCTION

Lifetimes or oscillator strengths of excited states of atoms and molecules have traditionally been measured through a determination of transition probabilities. The most reliable of these techniques is probably the Hook¹ method which yields, under favourable conditions, oscillator strengths to 10-20% accuracy. Common to these methods is the requirement that the partial pressure of the absorber must be accurately known. If the absorption occurs from the ground state of a stable gaseous atom this may present no problem. If, however, the absorption is produced by atoms or molecules of low vapor pressure or by an unstable molecule it is very difficult not to make large errors in determining the number of absorbers present. More recent techniques such as the phase-shift and delayed coincidence methods² do not suffer from the above shortcomings but do require fast "gates" with risetimes shorter than the excited state lifetime under consideration or other sophisticated electronics. Since in many cases lifetimes are of order 10^{-8} seconds or shorter, it is again easy to make errors of considerable magnitude. The use of zero-field level crossing to determine lifetimes suffers from none of these limitations and has been used to measure lifetimes of many atomic states and more recently to measure excited state lifetimes of NO⁴, OH⁵, and CS⁶.

An energy level diagram for the observed singlet states of molecular hydrogen is shown in FIG.1. The levels shown are the lowest vibrational, rotational levels of each electronic state. This thesis concerns itself primarily with the $3d^1\Sigma$ ($v=0$) $J=1$, 2, and 3 state lifetimes. The light observed arises from the transitions $R(0)$, $R(1)$, and $R(2)$ of the $(0,0)$ band of the $3d^1\Sigma \rightarrow 2p^1\Sigma$ system corresponding to the transitions



respectively.

A more detailed energy level diagram for these states is shown in FIG.2. The transitions observed in this thesis are marked with arrows.

The electronic portion of the wave function of these states ought to resemble those of the atomic Helium 3D states hence we expect lifetimes of the same order of magnitude, or roughly 10^{-8} seconds⁷.

Also observed were several $3K^1\Sigma \rightarrow 2p^1\Sigma$ transitions and a $3d^1\Pi \rightarrow 2p^1\Sigma$ transition. Information obtained on these states is contained in Appendix III.

The Hanle Effect

In 1922 Rayleigh⁸ discovered that the 2537°A line of mercury excited by resonance radiation, was polarized if

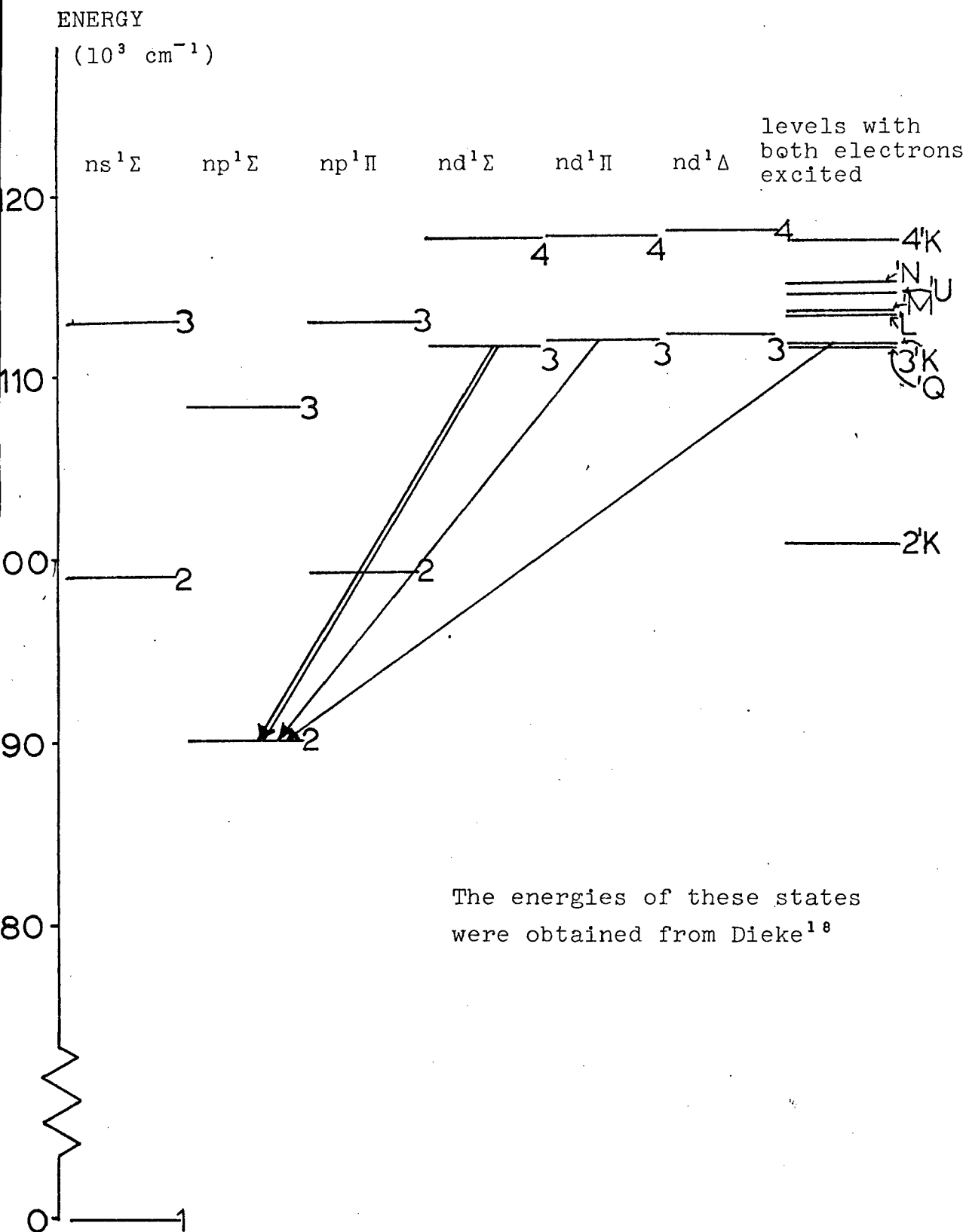
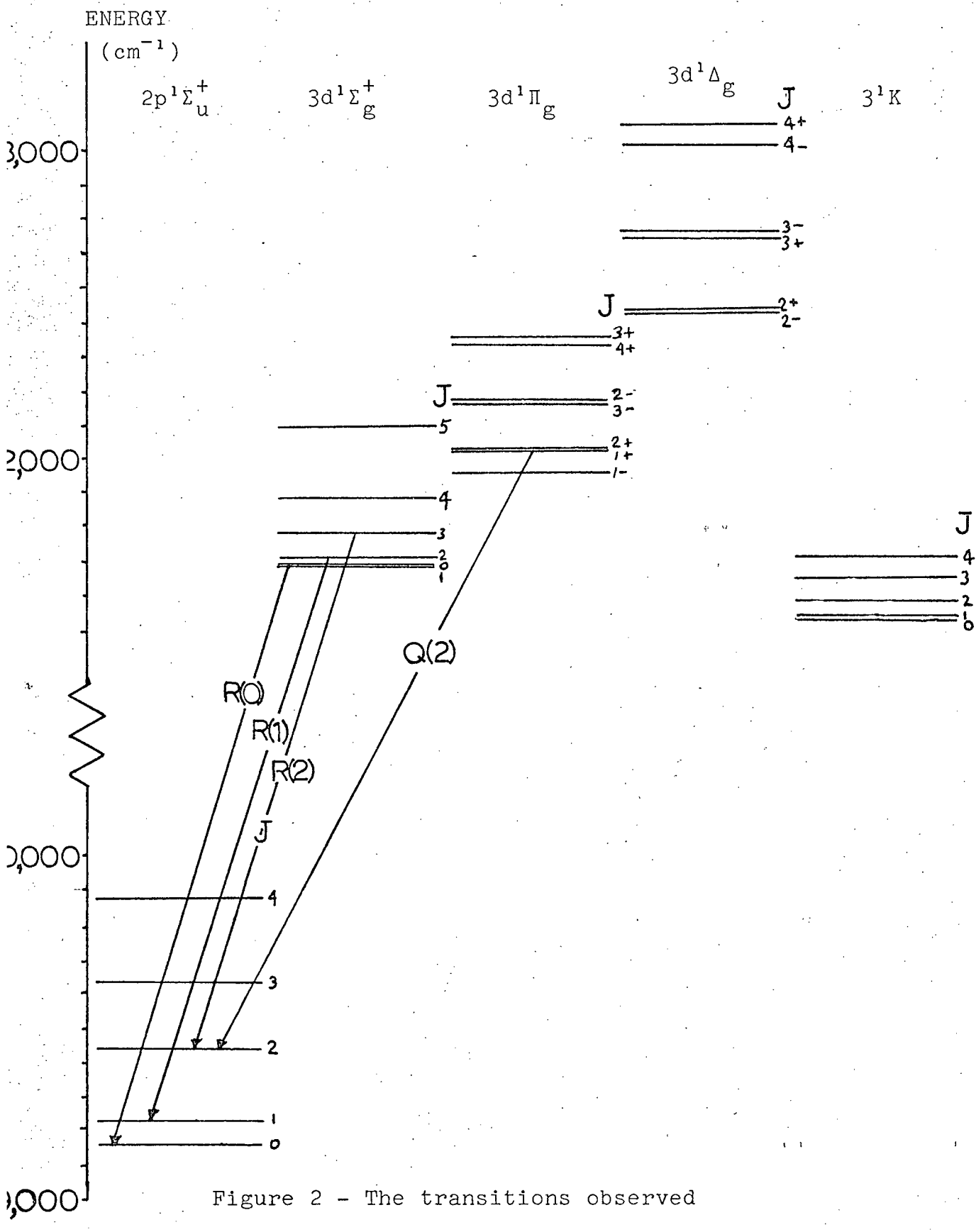


Figure 1 - The singlet states of hydrogen (H_2)



viewed at right angles to the exciting beam. Wood⁹ and Ellet¹⁰ investigated this effect further and found that at low pressures, in the absence of a magnetic field the emitted radiation was almost completely polarized with its electric vector parallel to that of the exciting light. Small magnetic fields in certain directions were found to decrease the degree of polarization. The addition of foreign gases was also found to decrease the polarization. Hanle¹¹, performing a more thorough investigation found that the application of a magnetic field perpendicular to the exciting light along the direction of observation not only decreased but also rotated the plane of polarization of emitted light. Breit¹² explained the effect in classical terms and showed that the degree of polarization, P, is given by the expression

$$\frac{P(H)}{P(0)} = \frac{1}{1 + \left(\frac{geH\tau}{mc}\right)^2} \quad (1)$$

where $P = \frac{I_{||} - I_{\perp}}{I_{||} + I_{\perp}}$, $I_{||}$ is the intensity of light with electric vector along the electric vector of the exciting beam and I_{\perp} that with perpendicular polarization, H is the applied magnetic field, τ is the mean radiative lifetime, $\frac{ge}{2mc}$ is the magnetic moment of the atom. A condensed version of the classical theory is given in § 2.2.

By plotting $P(H)$ we may then easily obtain the product $g\tau$, from eq.(1), and an independent measurement of g yields the radiative lifetime τ .

A more complete account of the early work on polarization of resonance radiation is given by Mitchell and Zemansky¹³.

The Hanle effect is a special example of "level-crossing", the appearance of interference effects when two states are degenerate to within their natural linewidth.

Electron Impact Polarization

Light emitted from atoms excited by low energy (~20 e.V.) electrons will in general also exhibit polarization relative to a direction along the electron beam.

Measurements of polarization were made for a number of atoms by several workers from 1925 to 1935¹⁴. The polarization in general depends on the incident electron energy in a complicated manner, and no adequate theory has yet been devised. The depolarization of light emitted by helium excited by slow electrons, in response to a magnetic field has been observed by Pebay-Peyroula et al¹⁵. The signals have the same magnetic field and lifetime dependence, given by eq.(1), as those produced by optically excited atoms. Descourbes¹⁶ also reports non-zero field level-crossing in the 3P states of He using electron excitation. Polarization of light emitted from H₂ triplet states excited by electron impact has been reported by Patrick Cahill et al¹⁷.

In this work, the radiative lifetimes of the

$3d^1\Sigma$ $v=0$ $J=1$, 2, and 3 rotational states of molecular hydrogen have been measured by zero field level-crossing using electron impact to excite the states in a manner similar to that Pebay-Peyroula et al¹⁵. These lifetimes have not been previously measured and should provide a check on wave functions calculated for these levels.

A brief, very readable review of lifetime measurements is given by Stroke⁹.

Notation and Symbols

The only major departure from the conventional symbols are those used in denoting the various states. Conventionally, " refers to the lower state and ' refers to the upper state in a transition. In this thesis we add to this convention that ground state quantum numbers are unprimed. J is the total angular momentum exclusive of nuclear spin and v is the vibrational quantum number.

Some ambiguity may also be encountered between \mathbf{g} , the polarization vector of an emitted photon and $g=g_J$, the Landé g-factor for a state; the latter will nearly always be accompanied by μ_0 or its equivalent, $\frac{e}{2mc}$.

CHAPTER II

THEORY

§2.1 Introduction

In this chapter we will discuss first the Hanle effect analogue in classical terms. Following this the quantum mechanical description of the effect usually referred to as level-crossing, will be presented. The theory given will follow the treatment of Franken¹⁹ quite closely.

Next we will consider the structure of the ground states and the $3d^1\Sigma$ levels of the hydrogen molecule. The transitions $1s^1\Sigma \rightarrow 3d^1\Sigma$ will be discussed in terms of ground state populations and allowed electric multipole transition moments.

Finally we will attempt to describe the relevant portions of the excitation mechanism.

§2.2 The Magnetic Field Dependence of Polarization in Classical Terms

In order to discuss the Hanle effect classically we replace our molecule by an electric dipole which possesses an angular momentum \underline{L} perpendicular to the dipole axis and a magnetic moment $\underline{\mu} = \mu \underline{L}$.

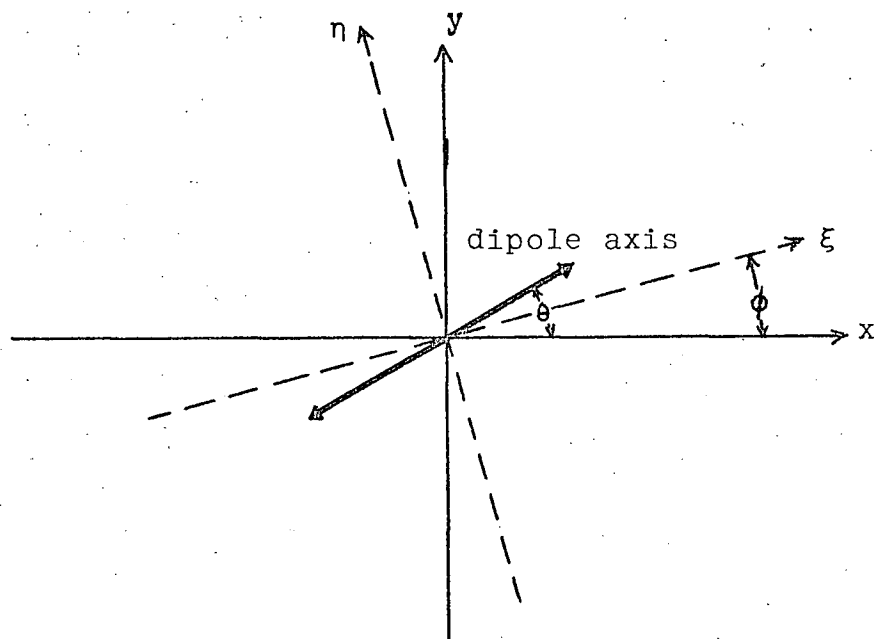


Figure 3 - Hanle effect co-ordinate system

Further, we suppose that at some time t_1 the dipole is set into oscillation with angular frequency ν . The dipole then emits radiation with its electric vector parallel to the dipole axis which at time t is at some angle $\theta(t)$ to the x -axis. In the absence of any torques on the dipole, $\theta(t)=\theta(0)=0$. If however a magnetic field $\underline{H}=\underline{H}_z \hat{k}$ is placed along the z -axis, the dipole precesses about the z -axis with angular velocity $\omega=\mu H$ and $\theta(t)=\mu H(t-t_1)$. The amplitude of radiation is radiation damped with a time constant 2τ . Thus an observer looking along the z -axis, having a reference system ξ, η, z where ξ and η are inclined at angle ϕ to x and y respectively, will observe a time dependent electric field with components:

$$E_\xi(t) = A_0 \cos[\omega(t-t_1)-\phi] e^{-i(vt+\delta)} e^{-\frac{t-t_1}{2\tau}}$$

$$E_\eta(t) = A_0 \sin[\omega(t-t_1)-\phi] e^{-i(vt+\delta)} e^{-\frac{t-t_1}{2\tau}}$$

or the intensities of radiation with electric vector along the ξ and η axes:

$$\begin{aligned} I_\xi(t) &= I_0 \cos^2[\omega(t-t_1)-\phi] e^{-\frac{t-t_1}{\tau}} \\ I_\eta(t) &= I_0 \sin^2[\omega(t-t_1)-\phi] e^{-\frac{t-t_1}{\tau}} \end{aligned} \quad (2)$$

Now, if our observer does not differentiate light emitted in the interval (t_1, t_1+T) where $T \gg \tau$, the intensities observed are

$$I_\xi = \int_{t_1}^{t_1+T} I_\xi(t) dt \approx \int_{t_1}^{\infty} I_\xi(t) dt$$

$$I_\eta = \int_{t_1}^{t_1+T} I_\eta(t) dt \approx \int_{t_1}^{\infty} I_\eta(t) dt$$

The polarization $P(\phi, H)$ is then $\frac{I_\xi - I_\eta}{I_\xi + I_\eta}$, or

$$P(\phi, H) = \frac{\int_{t_1}^{\infty} \{\cos^2[\omega(t-t_1)-\phi] - \sin^2[\omega(t-t_1)-\phi]\} e^{-\frac{t-t_1}{\tau}} dt}{\int_{t_1}^{\infty} e^{-\frac{t-t_1}{\tau}} dt}$$

performing the integration,

$$P(\phi, H) = \frac{1}{1+(2\omega\tau)^2} [\cos 2\phi - 2\omega\tau \sin 2\phi] \quad (3)$$

and substituting $\omega = \mu H$

$$P(\phi, H) = \frac{1}{1+(2\mu H \tau)^2} [\cos 2\phi - 2\mu H \tau \sin 2\phi]$$

For the special case of $\phi=0$ this reduces to

$$P(H) = \frac{1}{1+(2\mu H \tau)^2}$$

a sketch of this shape is shown in FIG. 4.

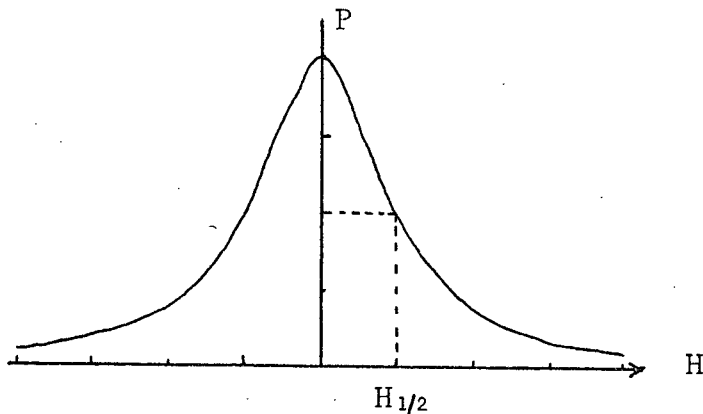


Figure 4 - Polarization for $\phi=0$

It should be noted that when $\frac{P(H)}{P(0)} = 1/2$ the "lifetime" τ of the oscillator is given by $\tau = \frac{1}{2\mu H_{1/2}}$

For the case $\phi = \pi/4$

$$P(H) = \frac{-2\mu H \tau}{1+(2\mu H \tau)^2}$$

yielding the curve shown in FIG 5.

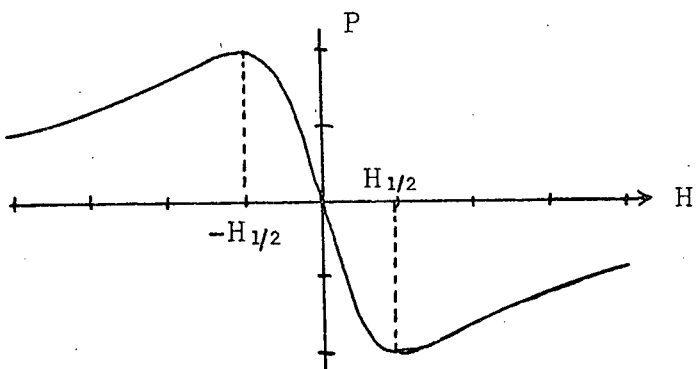


Figure 5 - Polarization for $\phi = \pi/4$

This curve not only yields the lifetime but also the sign of the magnetic moment of the oscillator.

From eq.(3) we may also see that the direction of polarization rotates with increasing magnetic field, for P takes on its maximum value at a given magnetic field for an angle ϕ such that $\frac{dP}{d\phi} = 0$, i.e.

$$-2\sin 2\phi - 4\mu H\tau \cos 2\phi = 0, \text{ or}$$

$$\phi = \tan^{-1}(2\mu H\tau)$$

Up to this point we have tacitly assumed that our radiating system was composed of only a single oscillator set into motion along the x -axis at time t_1 . Actually we have N oscillators excited at random times t_j and having their initial motions on axes distributed about the x -axis.

The intensities seen by the observer due to n oscillators incoherently excited along the x -axis and decaying during time $T \gg \tau$ is just

$$I_\xi(t) = \sum_{j=1}^n \int_t^T I_\xi(t_j, t) dt \approx n \int_{t_j}^\infty I_\xi(t_j, t) dt$$

$$I_n(t) = \sum_{j=1}^n \int_t^T I_n(t_j, t) dt \approx n \int_{t_j}^\infty I_n(t_j, t) dt$$

which again leads to equation(3) for the polarization.

We now consider an oscillator excited in the $x-y$ plane with its axis at an angle θ_0 to the x -axis.

The polarization seen by the observer is then

$$P(\phi, \theta_0, H) = \frac{1}{1 + (2\mu H \tau)^2} [\cos 2(\phi - \theta_0) - 2\mu H \tau \sin 2(\phi - \theta_0)]$$

Summing now over n oscillators with initial axes symmetrically distributed about the x-axis in the x-y plane

$$\begin{aligned} P(\phi, H) &= \sum_{j=1}^n P(\phi, \theta_j, H) = \\ &= \frac{P_o}{1 + (2\mu H \tau)^2} [\cos 2\phi - 2\mu H \tau \sin 2\phi] \end{aligned} \quad (4)$$

$$\text{where } P_o = \frac{1}{n} \sum_{j=1}^n \cos 2\theta_j, \quad |P_o| \leq 1$$

Thus although the polarization has been decreased, the polarization shows the same field dependence.

Similarly it can be shown, although more tediously, that for a symmetric distribution of oscillators in the x-y plane the maximum polarization is again only decreased but no change in its magnetic field dependence occurs.

It should be clear that the perturbation which excited the oscillator should be short in duration compared to the radiative lifetime for the above derivation to apply. The time involved in the collision is of order 10^{-14} seconds thus this should be well satisfied.

The oscillator should also not be subject to re-orientation or interruption by collision with its neighbors, or a change in the polarization will again result. To apply the preceding theory to an atomic or molecular

system we need merely evaluate the magnetic moment $\mu = g\mu_0 L$ where μ_0 is the Bohr magneton $= \frac{e}{2mc}$. Thus finally:

$$P(\phi, H) = \frac{\mu_0}{1 + (\frac{geH\tau}{mc})} z [\cos 2\phi - \frac{geH\tau}{mc} \sin 2\phi] \quad (5)$$

§ 2.3 Quantum-Mechanical Description of Level Crossing

In 1933 Breit²⁰ derived a quantum mechanical expression, the "Breit formula", for the radiation rate from coherently excited, nearly degenerate states of a system. This was largely ignored until 1958 when Franken et al²¹ reported the measurement of the fine structure in some Helium levels using level-crossing. They re-derived the "Breit formula", under conditions of pulse excitations as well as excitation by white light.

Consider a "three" level system with ground state $|a\rangle$ and excited states $|b\rangle$ and $|c\rangle$ with the energy of $|a\rangle$ taken for convenience to be zero.

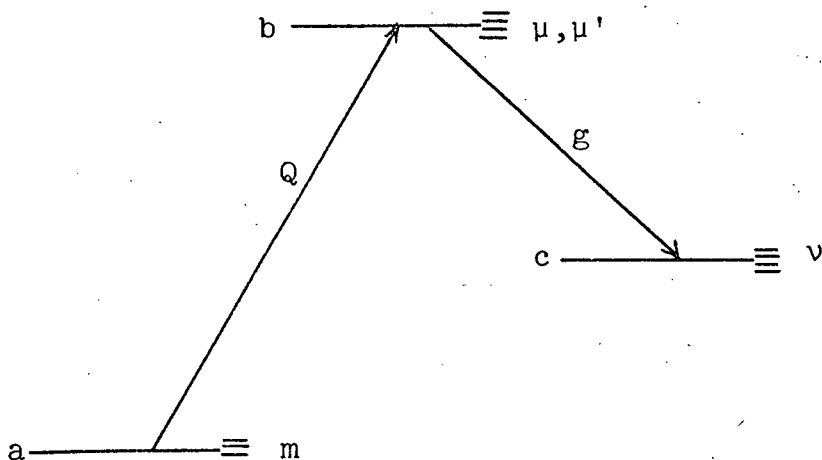


Figure 6 - "Three" level system

They have magnetic sublevels m , μ , and v , respectively.

i.e. We have the unperturbed states:

$$\begin{aligned} |a, J, m; t\rangle &= |a, J, m\rangle & m = -J, -J+1, \dots, J \\ |b, J', \mu; t\rangle &= |b, J', \mu\rangle e^{-(i\omega_\mu + \Gamma_b/2)t} & \mu = -J', -J'+1, \dots, J' \\ |c, J'', v; t\rangle &= |c, J'', v\rangle e^{-(i\omega_v + \Gamma_c/2)t} & v = -J'', -J''+1, \dots, J'' \end{aligned}$$

where $\omega_\alpha = \frac{E_\alpha}{\hbar}$, E_α is the energy of state α , and $\Gamma_\alpha = \frac{1}{\tau_\alpha}$

expresses the radiation damping of the state.

At time $t=0$, the atom is assumed to be in one of its ground states $|a, J, m\rangle$ when it is subjected to a pulse perturbation Q which may excite it to some of the states $|b, J', \mu\rangle$. The state vector of the system using first order perturbation theory is then at subsequent times:

$$|\chi_m; t\rangle = |a, J, m\rangle + \sum_{\mu} |b, J', \mu\rangle \langle b, J', \mu| Q |a, J, m\rangle e^{-(i\omega_\mu + \Gamma_b/2)t}$$

Now the states $|b, J', \mu\rangle$ are assumed capable of decaying to the states $|c, J'', v\rangle$ by emission of a photon of polarization g .

The rate at which this occurs is given by

$$R_{m, b, c}(Q, g, t) = \sum_v |\langle \chi_m; t | \underline{g} \cdot \underline{r} | c, J'', v \rangle|^2$$

Where $\underline{g} \cdot \underline{r}$ is the dipole moment operator. Since any one of the ground states m could have been excited we sum over m as well to obtain the total instantaneous emission rate of photons of polarization g at time t .

$$R_{bc}(Q, g, t) = \sum_{mv} |\langle \chi_m; t | \underline{g} \cdot \underline{r} | c, J'', v \rangle|^2$$

Substituting for $|\chi_m, t\rangle$ we obtain:

$$R_{bc}(Q, \underline{g}, t) = \sum_{m\nu} \sum_{\mu} e^{(i\omega_{\mu} - \Gamma_b/2)t} \langle b, J', \mu | Q | a, J, m \rangle \cdot \langle b, J', \mu | \underline{g} \cdot \underline{r} | c, J'', \nu \rangle^2$$

and expanding the square, this becomes

$$R_{bc}(Q, \underline{g}, t) = \sum_{m\mu\mu'} \sum_{\nu} e^{[i(\omega_{\mu} - \omega_{\mu'}) - \Gamma_b]t} Q_{\mu m} Q_{m\mu'} g_{\mu'} v g_{v\mu}$$

where $Q_{\alpha\beta} = \langle \alpha | Q | \beta \rangle$

$$g_{\alpha\beta} = \langle \alpha | \underline{g} \cdot \underline{r} | \beta \rangle$$

Now if we have N systems each subjected to an impulse at random times within the interval $(0, T)$ and observe the system for a time $T >> \frac{1}{\Gamma}$, the radiation rate observed becomes:

$$\begin{aligned} R_{bc}(Q, \underline{g}) &= N \int_0^T R_{bc}(Q, \underline{g}, t) dt \approx N \int_0^\infty R_{bc}(Q, \underline{g}, t) dt \\ &= N \sum_{m\mu\mu'} \sum_{\nu} \frac{Q_{\mu m} Q_{m\mu'} g_{\mu'} v g_{v\mu}}{\Gamma - i(\omega_{\mu} - \omega_{\mu'})} \\ &= N\Gamma \sum_{m\mu\mu'} \sum_{\nu} \frac{Q_{\mu m} Q_{m\mu'} g_{\mu'} v g_{v\mu}}{1 - i\tau(\omega_{\mu} - \omega_{\mu'})} \end{aligned} \quad (6)$$

This is the "Breit formula". Some of its implications are easily investigated.

- 1) If the various $|\mu\rangle$ and $|\mu'\rangle$ are well resolved (i.e. $|\tau(\omega_{\mu} - \omega_{\mu'})| >> 1$), the sum in the Breit formula (eq.(6)) reduces to just those terms for which $\mu = \mu'$

$$R_{bc}(Q, \underline{g}) \propto \sum_{m\mu\nu} |Q_{\mu m}|^2 |g_{\mu\nu}|^2 = R_o$$

this is just fluorescence with no interference terms.

2) If, however, $|\tau(\omega_\mu - \omega_{\mu'}, v)| \lesssim 1$ we obtain some interference terms as well, setting $A = Q_{\mu m} Q_{m\mu'} g_{\mu',v} g_{v\mu} = A(m, \mu, \mu', v)$

$$\begin{aligned}
 R_{bc}(Q, g) &= R_o + \sum_{m \neq \mu} \sum_{\mu' > \mu} \frac{A(m, \mu, \mu', v)}{1 - i\tau(\omega_\mu - \omega_{\mu'}, v)} \\
 &= R_o + \sum_{m \neq \mu} \sum_{\mu' > \mu} \frac{A(m, \mu, \mu', v)}{1 - i\tau(\omega_\mu - \omega_{\mu'})} + \frac{A^*(m, \mu, \mu', v)}{1 + i\tau(\omega_\mu - \omega_{\mu'})} \\
 &= R_o + \sum_{m \neq \mu} \sum_{\mu' > \mu} \frac{1}{1 + \tau^2(\omega_\mu - \omega_{\mu'})^2} \cdot \\
 &\quad \cdot \{A + A^* + i\tau(\omega_\mu - \omega_{\mu'}) (A - A^*)\} \quad (7)
 \end{aligned}$$

It will be shown in Appendix I that $A=0$ unless $\mu-\mu'=2$, it will also be shown that in this experiment A has the form $A=A_o e^{2i\phi}$, where ϕ is the angle g makes with the x-axis.

Then if the levels exhibit a linear Zeeman effect in a magnetic field $\omega_{b\mu} = \omega_b + \frac{geH}{2mc} H\mu$

$$\text{and } \omega_\mu - \omega_{\mu'} = \frac{geH}{mc}$$

Hence

$$\begin{aligned}
 R_{bc}(Q, g, \phi) &= R_o + \sum_{m \neq \mu} \sum_{\mu' > \mu} \frac{2A_o}{1 + \left(\frac{geH\tau}{mc}\right)^2} \cdot \\
 &\quad \cdot \{\cos 2\phi - \frac{geH\tau}{mc} \sin 2\phi\} \quad (8)
 \end{aligned}$$

The polarization P , with respect to the axis ξ is then

$$P = \frac{R_{bc}(Q, g, \phi) - R_{bc}(Q, g, \phi + \pi/2)}{R_{bc}(Q, g, \phi) + R_{bc}(Q, g, \phi + \pi/2)}$$

Substituting the expressions for R_{bc} from eq.(8),

$$\begin{aligned}
 P &= \frac{1}{1 + \left(\frac{geH\tau}{mc}\right)^2} \cdot \frac{2}{R_o} \sum_m \sum_{v>\mu} \sum_{\mu'>\mu} A_o(m, \mu, \mu', v) \\
 &\quad \cdot \{\cos 2\phi - \frac{geH\tau}{mc} \sin 2\phi\} \\
 &= \frac{P_o}{1 + \left(\frac{geH\tau}{mc}\right)^2} \{\cos 2\phi - \frac{geH\tau}{mc} \sin 2\phi\} \tag{9}
 \end{aligned}$$

$$P_o = \frac{2}{R_o} \sum_m \sum_{v>\mu} \sum_{\mu'>\mu} A_o(m, \mu, \mu', v)$$

Comparing eq.(9) with the expression for the polarization derived classically (eq.(5), §2.2) we see that, except for a difference in the definition of P_o , the two expressions are the same.

§2.4 The $3d^1\Sigma$ Levels of H_2

In the highly excited states of light molecules such as H_2 and He_2 , the rotation of the nuclei may be sufficiently rapid at even small rotational quantum numbers that the Born-Oppenheimer²² approximation, the resolution of the total eigenfunction into a product of electronic, vibrational and rotational eigenfunctions, is no longer valid. We must describe the states in terms of the coupling between the internuclear axis and the electronic motion, and the coupling of electronic motion with the axis of rotation.

The various types of coupling in a molecule are described by Herzberg²³ and usually referred to as Hund's case a, b, c, d, and e in their extreme limits. The $3d^1\Sigma$

states of H_2 can be well described as having a coupling between Hund's case b and d. A treatment of this coupling was given by Davidson²⁴ when he analyzed these states. A more recent discussion of coupling intermediate between case b and d has been given by Von I. Kovács and A. Budó²⁵ who also derived the Zeeman splittings expected in a magnetic field.

The application of this theory to the $3d^1$ levels of H_2 is found in Appendix II.

In the next section we will see that the excitation perturbation may be expanded in electric multipole moments. It is convenient here to establish which of these moments will have zero, and which will have non-zero expectation values between the ground state $1s^1\Sigma$ and the $3d^1\Sigma$ state.

As is well known a molecule composed of atoms with nuclear spins I_1 and I_2 will have a resultant nuclear spin $I = I_1 + I_2, I_1 + I_2 - 1, \dots, |I_1 - I_2|$. For H_2 this means that $I = 1$ or 0 . The rotational levels alternately have these values of I ; in particular for the $^1\Sigma_g^+$ states, even J states have $I = 0$ and odd J states have $I = 1$. The transition from a state with $I = 0$ to one with $I = 1$ is an exceedingly improbable event having in the pure liquid transition probability of order 10^{-7} sec.⁻¹. Ruling out this transition we have then the selection rule

$$J' = J, J \pm 2, J \pm 4, \dots$$

The parity of the states specifies which of the multipole moments are zero between state J and J' . We note that Σ^+ states have parity $(-1)^J$ and that the electric 2ℓ -pole moment $Q^{(\ell)}$ has parity $(-1)^\ell$. It is then easy to see that $\langle \alpha, J | Q^{(\ell)} | \beta, J \pm 2n \rangle$ where n is an integer, is zero unless ℓ is an even integer; furthermore, from the properties of spherical harmonics one can show that:

$$\langle \alpha, J | Q^{(\ell)} | \beta, J \pm 2n \rangle = 0$$

unless $2n \leq \ell$, and in the case $n=0$, $\ell > 2J$, so that for the first nonvanishing electric multipole moment between ${}^1\Sigma_g^+$ states we have the electric quadrupole moment $Q_{\alpha\beta}^{(2)}$.

In the discussion of level crossing we always assumed that the ground state $|\alpha, J\rangle$ was specified and for atomic problems this is usually so. When considering molecules at thermal equilibrium we find that at room temperature not one, but several rotational states are populated with their populations given by the Maxwell-Boltzmann distribution law, i.e. the population N_J of the state J is given by

$$N_J = N f_J e^{-\frac{E_J}{kT}}$$

where f_J is the degeneracy of the state = $(2J+1)(2I+1)$

E_J is the energy of the state J

k is Boltzmann constant = $1.38\dots \times 10^{-16}$ ergs/ $^{\circ}\text{C}$

T is the absolute temperature

N is a normalizing factor

The relative ground state populations at room temperature and those when lowered to 80°K remembering the ortho-para conversion restriction are tabulated in Table I.

J	at 292°K	at 80°K	I
0	.132	.2491	0
1	.663	.7492	1
2	.115	.0017	0
3	.086	7×10^{-6}	1
4	.004		0

Table I - Relative Populations of the First Few Rotational Levels of Hydrogen at Thermal Equilibrium.

It can be seen that at room temperature the $J'=2$ state will, under the previous selection rules, be excited having either the $J=0$ and $J=2$ states as ground state. When the temperature is lowered to 80°K however, no such ambiguity exists any more and only the $J=0$ state will serve as ground state.

§25 The Excitation Matrix Elements Q

In order to apply the Breit formula we must find an expression for the perturbation matrix elements $Q_{\alpha\beta}$. Even though the laws governing electron-atom collisions at non relativistic energies are completely known, the calculation of low energy scattering cross sections is extremely complex and has only been attempted for the simplest atomic cases²⁶.

Referring to eq.(9), §2.3, it should be noted that so long as $P_0 \neq 0$ and is independent of the magnetic field, its numerical value is irrelevant to the determination of τ . Therefore, digressing somewhat, we will consider what can be said of P_0 in the absence of a magnetic field. The level crossing formulism is not convenient for this; instead, the excitation and decay are now considered as two independent processes. We consider first the decay.

To be specific let us consider a hypothetical transition $J=1 \rightarrow J=0$ observed along an axis perpendicular to the axis of quantization (z-axis). The transitions thus observed are $\Delta m = \pm 1$ and $\Delta m = 0$ having polarizations perpendicular and parallel to the z-axis respectively. If all three states $m=0$, $+1$ and -1 of the $J=1$ level are equally populated the emitted light should show no polarization since the z-axis was arbitrarily chosen. If however, the excitation mechanism populates the state $m=0$ differently from the states $m=\pm 1$, either the $\Delta m = \pm 1$ or the $\Delta m = 0$ transitions

dominate as the source of emitted radiation and hence the light will be polarized along or perpendicular to the z-axis.

When the populations of different $|m|$ are unequal the molecules are said to be aligned and in general the radiation emitted will show some polarization with respect to the axis of quantization. Thus to obtain a $P_0 \neq 0$ it is only necessary that the excitation align the molecules. If the colliding electron has sufficiently low energy it is easy to show that alignment occurs.

Let the electron travel along the z-axis with momentum $\underline{P} = \hat{P}\underline{k}$, and be scattered inelastically by the molecule at a distance R . The angular momentum of the electron about the scattering centre is then $\underline{\ell} = \underline{P} \times \underline{R}$, in particular $\ell_z = 0$; after the collision we assume that the energy of the electron is sufficiently small that $|\underline{\ell}'| = |\underline{P}' \times \underline{R}| \ll h$, i.e. the energy of the scattered electron $E' = \frac{P'^2}{2m} \ll \frac{h^2}{2mR^2}$, then $\ell'_z = 0$. Thus for the collision $\Delta \ell_z = 0$ and conservation of angular momentum for the whole system then implies that $\Delta J_z = 0$. Thus if the collision increases J , alignment of the upper-state levels occurs. If $\Delta J_z < 0$ we need as an extra condition that the scattering cross sections for different $|m|$ be non-equal.

The condition on the scattered electron energy (above) is quite stringent, for $R = 5\text{\AA}$ and $\ell' \leq \frac{h}{10}$ for instance $E \leq \frac{h^2}{2mR^2 \times 10^2} \approx 0.15\text{e.V.}$, so that even in cases

where the ground state angular momentum is zero and the polarization can be uniquely predicted it is not expected to be realized experimentally where much greater energy excesses occur.

When P_0 is not independent of the magnetic field, as will be the case for non-zero field level crossings, the matrix elements A_0 must be computed as a function of magnetic field. For this reason as well as for the sake of completeness, the relative matrix elements for excitation to the various μ, μ' will be considered. No adequate theory exists and various approximations such as the Born approximation are valid only at energies above a few hundred e.v. Nevertheless, because of its relative simplicity and for lack of a much better theory, the Born approximation will be used. It is expected that although absolute cross-sections so obtained will be highly erroneous, relative matrix elements $Q_{m\mu}, Q_{m\mu'}$, will be at least qualitatively correct. These matrix elements are used explicitly only in the discussion in §5.2 where the effect of hyperfine splittings of the order of the natural linewidth, will be considered.

We let \underline{p} and \underline{p}' be the momenta of the incident electron before and after the collision. Then for transition probability amplitude, $Q_{\beta\alpha}$, from a state α to β , whose energies differ by $E_{\alpha\beta}$, we take in accordance with the Born approximation²⁷;

$$Q_{\alpha\beta}(p, q) \propto \langle \beta | \int U e^{-q \cdot r_e} dr_e^3 | \alpha \rangle$$

$$\text{where } \underline{q} = \frac{\underline{p}' - \underline{p}}{\hbar}, \quad |\underline{q}| = \sqrt{\frac{2mE_{\alpha\beta}}{\hbar^2}}$$

r_e is the incident electron's position vector

U is the interaction potential; taken to be the electrostatic interaction

$$U(\{R_n, R_e\}, r_e) = \sum_{e,n} \frac{e^2}{|r_e - R_n|} - \frac{e^2}{|r_e - R_e|}$$

with R_n = the position vector of nucleus n

$\{n\}$ = the set of nuclei

R_e = the position vector of electron e

$\{e\}$ = the set of molecule's electrons

m is the mass of electron

Carrying out the integration over r_e we obtain

$$Q_{\beta\alpha} \propto \langle \beta | \sum_{i \in \{e, n\}} e^{-iq \cdot R_i} | \alpha \rangle$$

We expand the exponential in a power series and obtain

$$Q_{\beta\alpha} = Q_{\beta\alpha}^{(1)} + \frac{Q_{\beta\alpha}^{(2)}}{2} + \frac{Q_{\beta\alpha}^{(3)}}{6} + \frac{Q_{\beta\alpha}^{(4)}}{24} + \dots \quad (10)$$

Where

$$\frac{e}{(iq)^l} Q_{\beta\alpha}^{(l)} = \langle \beta | e \sum_i \left| \frac{q}{|q|} \cdot R_i \right|^l | \alpha \rangle$$

or the electric $2-l$ pole moment in the \underline{q} direction between the states β and α .

$(Q_{\beta\alpha}^{(0)} = \langle \beta | l | \alpha \rangle = \delta_{\alpha\beta}$ from orthogonality of $|\alpha\rangle$ and $|\beta\rangle$)

For $E \approx 14$ e.V. and $\underline{R}_i \approx 5 \times 10^{-8}$ cm $|\underline{q}^\ell \cdot \underline{R}_i^\ell| \leq 1$

so that this series expansion, eq.(10), converges approximately as $\frac{1}{n!}$. We have seen in §2.4 that for our states $Q_{\beta\alpha}^{(1)} = Q_{\beta\alpha}^{(3)} = 0$, hence we may approximate $Q_{\beta\alpha}$ by:

$$\frac{Q_{\beta\alpha}^{(2)}}{2} \approx \langle \beta | e \cdot \sum_{i \in \{n, e\}} \left(\frac{\underline{q}}{|\underline{q}|} \cdot \underline{R}_i \right)^2 | \alpha \rangle$$

For a specified \underline{q} this completes our problem, but unfortunately \underline{q} is not specified unless $\underline{p}' = 0$, i.e. $\frac{\underline{p}}{2m} = E_{\alpha\beta}$, so that we must make a further approximation. We expect that so long as \underline{p}' is small, \underline{q} will lie approximately along $-\underline{p}$; setting $\underline{k} = \frac{\underline{p}}{\hbar}$, $\underline{k}' = \frac{\underline{p}'}{\hbar}$, $\underline{q} = \underline{k}' - \underline{k}$

The directions \underline{q} takes are easily seen from the following diagram (FIG.7).

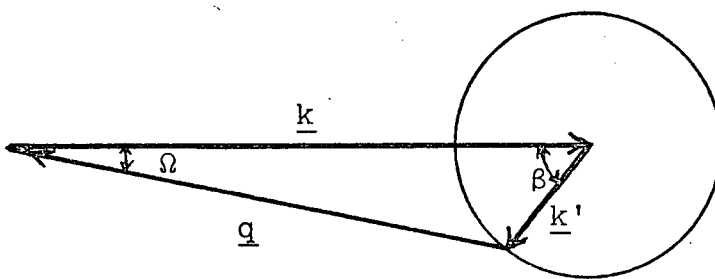


Figure 7 - The Scattering Angle Ω

By conservation of energy \underline{k}' is restricted in magnitude to:

$$|\underline{k}'| = |\underline{k}| - \sqrt{\frac{2mE_{\alpha\beta}}{h^2}}$$

The maximum angle \underline{q} makes with $-\underline{k}$ is then $\Omega = \sin^{-1} \frac{\underline{k}'}{|\underline{k}|}$.

Thus for a 16 e.V. incident electron scattered with an energy of 2 e.V., $|\Omega| \leq \sqrt{\frac{2}{16}} \approx 20^\circ$; if the electron is scattered so that \underline{k}' is spherically symmetrically distributed, $\langle \underline{q} \rangle = -\underline{k}$ i.e. $\langle \Omega \rangle = 0$, and

$$\begin{aligned}\langle \sin^2 \Omega \rangle &= \frac{1}{2\pi} \int_0^{2\pi} \frac{\underline{k}'^2 \sin^2 \beta d\beta}{(\underline{k} - \cos \beta)^2} \\ &= \frac{1}{2\pi} \int_0^{2\pi} \frac{\underline{k}'^2 \sin^2 \beta d\beta}{\underline{k}^2} - O\left(\left(\frac{\underline{k}'}{\underline{k}}\right)^4\right) \\ &= \frac{\underline{k}'^2}{2\underline{k}^2} - O\left(\left(\frac{\underline{k}'}{\underline{k}}\right)^4\right)\end{aligned}$$

hence, using the same \underline{k} and \underline{k}' as above,

$$\langle \sin^2 \Omega \rangle < .06$$

leading to

$$\sqrt{\langle \Omega^2 \rangle} < 14^\circ.$$

Although this is not an impressively small dispersion we shall assume in deriving the Breit formula matrix elements that $\frac{\underline{q}}{q} = -\frac{\underline{k}'}{\underline{k}} = \hat{i}$ and hence the matrix elements $Q_{\beta\alpha}$ are proportional to those of the electric quadrupole moment $Q_{xx}^{(2)}$. Specific formulae and the application of these formulae to the transitions observed are found in Appendix I.

CHAPTER III

EXPERIMENTAL DETAILS

§3.1 Experimental Arrangement

In view of the discussion in the preceding chapter the essentials of this experiment should consist of a discharge excited by 15 - 20 e.V. electrons travelling along the x-axis, a homogeneous variable magnetic field in the discharge region, a filter for resolving a given transition, and a device for detecting and measuring polarization. The basic apparatus is shown in FIG. 8; no attempt at scaling or realism was made in this sketch.

A discharge cell is placed between a pair of capacitor plates each parallel to the y-z plane. Between these plates a radio-frequency electric field of the form $\underline{E} = (E_0 \cos \omega t) \hat{i}$ causes free electrons to oscillate in the $\pm x$ direction with the appropriate energy. Centered about the discharge are 2 pairs of Helmholtz coils; one to cancel the vertical component of the earth's magnetic field, the other to produce a field $\underline{H} = H_k \hat{k}$. Light emitted in the z direction is focussed by a pair of lenses onto the entrance slit of a monochromator to spectrally resolve the transition of interest. Light appearing at the exit slit of the monochromator falls on a photomultiplier whose output is fed into the signal channel of a lock-in amplifier.

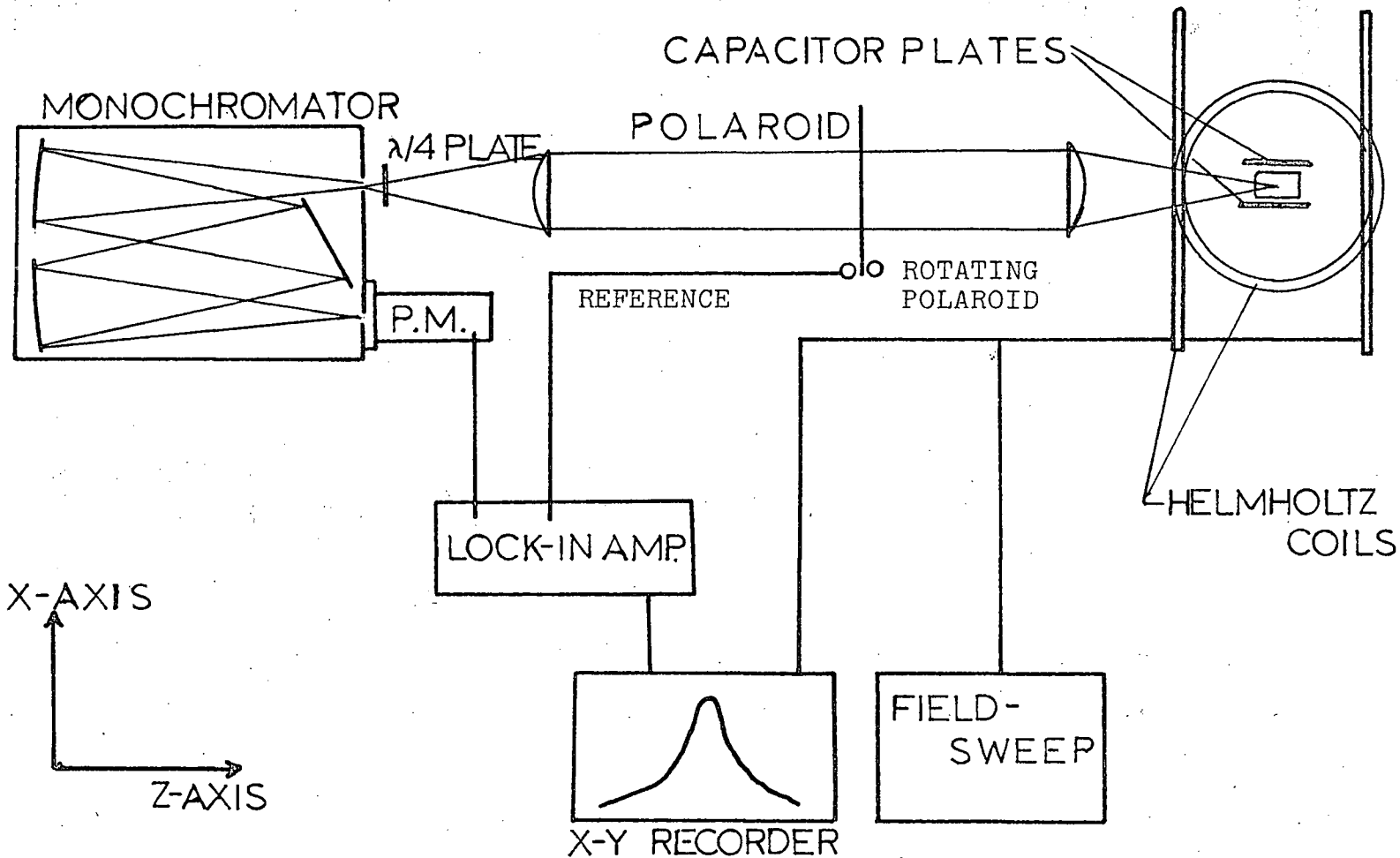


Figure 8 - The Apparatus

The light passing between the two lenses is passed through a polaroid, with its plane perpendicular to the beam, which is rotated about the x-axis. The polarized component of light is thus modulated at twice rotational frequency. A small light and photodiode placed at the rim of the polaroid, one on either side provide a reference signal for the lock-in amplifier. The output of the lock-in amplifier is connected to the y-channel of the x-y recorder. The x-channel is controlled by the voltage across Helmholtz coils producing the field $\underline{H} = \hat{H}k$. These coils are driven by a pair of power supplies and an amplifier whose output is slowly swept to produce fields of the form $H = H_0 + H_1 t$ where $H_0 \approx -10$ gauss and $H_{\max} \approx +10$ gauss.

A quarter wave plate is placed in the beam with its fast axis at 45° to the x-axis in the x-y plane just before the entrance slit of the monochromator to eliminate the effect of the monochromator transmitting y polarized light preferentially over x polarized light.

To ensure that the effects observed were not due to the R.F. fields, the experiment was performed using frequencies $f=180$ MHz and later with $f=450$ MHz and corresponding changes in electric fields.

§ 3.2 The Discharge

The discharge apparatus consists of a cylindrical pyrex discharge cell of 5 cm diameter and 2.5-3 cm length

connected to the vacuum system by two 1 cm O.D. pyrex tubes as shown in FIG. 10. The ends of the discharge cell are slightly convex outwards to provide mechanical strength against air pressure. A circular brass plate of 7 cm diameter is placed at either end so that it extends about 1 cm beyond the edges of the cell. The planes of the plates are parallel to the axis of observation. The output of a radio frequency transmitter is coupled to these plates in a manner described in §3.5.

The cell and plates are shown full scale in FIG. 9 below. For convenience the co-ordinate axes used throughout the discussion are also shown:

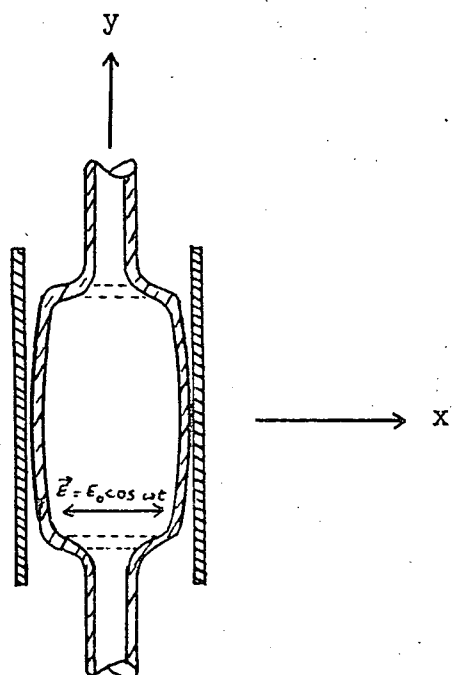


Figure 9 - Cross-Section of Discharge
Cell and Capacitor Plates

The discharge is assumed to consist of a dilute gas of neutral molecules and a much smaller number of free electrons. The motion of the electrons in a radio-frequency electric field, assuming a complete absence of collisions and zero magnetic field is governed by:

$$m\ddot{x} = eE_0 \cos \omega t$$

$$x = \frac{eE_0}{m\omega^2} \cos \omega t$$

and the kinetic energy K.E.:

$$\begin{aligned} \text{K.E.} &= \frac{1}{2} m x^2 \\ &= \frac{1}{2m} \left(\frac{eE_0}{\omega} \right)^2 \sin^2 \omega t \end{aligned}$$

The application of a small magnetic field $\underline{H} = H \hat{k}$ yields, still assuming no collisions or damping,

$$m\ddot{x} = eE_0 \cos \omega t - eHy$$

$$m\ddot{y} = eHx$$

solving these equations:

$$x(\omega t) = -\frac{eE_0}{m} \frac{1}{\omega^2 - v^2} \cos(\omega t)$$

$$y(\omega t) = \frac{v}{\omega} x(\omega t + \pi/2), \quad v = \frac{eH}{m}$$

in other words, the electron moves on an ellipse whose ratio of major to minor diameter is $\frac{\omega}{v}$.

In order for the above to meet the conditions of the discharge cell, 3 conditions must be satisfied:

- 1) elastic collisions of electrons with neutral

molecules ought to occur sufficiently infrequently.

This may be restated as: the mean free path of the electron should exceed the amplitude of its motion considerably.

- 2) collisions of electrons with the walls of the discharge cell must also be rare events. This merely means that any dimension of the discharge cell ought to exceed considerably the amplitude of electron motion.
- 3) electrons must be sufficiently energetic to ionize the occasional molecule in order to make up for electrons lost by recombination and sustain the discharge.

The third condition implies that we must give our electrons a maximum kinetic energy or order 20 e.v. Table 2 lists some of the properties of the motion of the electrons in an electric field oscillating at frequency $f = 2\pi\omega$.

Condition 2 (above) is clearly satisfied for all the frequencies tabulated in Table 2 in a discharge cell of the size used. In order to see how well the first condition is satisfied we compute the mean free path, L between molecules of cross-section σ , distributed with a density ρ :

$$L = \frac{1}{\rho\sigma}$$

frequency ($\times 10^6$ Hz)	E_0 required to produce $K.E._{max} = 20 e.V.$	amplitude of electron motion (major diameter)	minor axis to major axis ratio in 10 gauss magnetic field
100	100 V/cm	4 mm	.07
200	200 V/cm	2 mm	.035
500	500 V/cm	0.8 mm	.014

Table II - Properties of Electron Motion in an
R.F. Electric and D.C. Magnetic Field

Then at a density of $1.77 \times 10^{15}/\text{cm}^3$ (.05 mm Hg at room temperature) and assuming a cross-section of $\sim 10 \text{ \AA}^2$ we find the mean free path $L \approx 6 \text{ mm}$. Thus at these densities the foregoing description of the electrons' motion can at best be expected to be qualitative.

§3.3 The Optical System

As shown in FIG. 8, a pair of plano-convex lenses of focal length $F = 20 \text{ cm}$ each and aperture $F/6$, are placed, one at its focal length from the discharge, the other at its focal length from the entrance slit of the monochromator, so that light originating at the centre of the discharge traverses the space between the lenses in a parallel beam and is focussed onto the entrance slit of the monochromator. Between the lenses a rotating polaroid is placed; the aperture of the polaroid is large enough not to constitute

a "stop" in the optical system. The rotating polaroid is shown in FIG. 16. At the wavelengths this experiment was performed (4930 \AA) the monochromator, an F/8 Spex 1 m instrument, has, when used in second order, a dispersion of $\sim 6 \text{\AA/mm}$, and a resolution of better than 0.1\AA . Slit-widths of 0.3 mm for both entrance and exit slits were used throughout, yielding a resolution of $\sim 2 \text{\AA}$. The monochromator was found to polarize incident light in a manner that varied with wavelength. At 4930 \AA it polarized light approximately 80% along the y-axis (parallel to the grating lines). As this leads to modulation of light intensity at the exit slit when unpolarized light is incident on the rotating polaroid, the monochromator must be made insensitive to polarization. This was accomplished by placing a quarter-wave plate with its fast (or slow) axis at 45° to the x- and y-axis. A variable wavelength quarter-wave plate described in §3.10 was produced for this purpose. Because it is not immediately obvious how the quarter-wave plate corrects for the monochromator polarization a brief theoretical treatment follows.

We consider an electromagnetic wave whose electric vector makes an angle θ with the x-axis, travelling along the z-axis. It falls on a polarizer rotating at angular frequency ω . The incident light has then an electric vector E with components E_x and E_y referred to the usual x, y, z reference system.

$$E_x = A_0 \cos \theta e^{i(kz-vt)}$$

$$E_y = A_0 \sin \theta e^{i(kz-vt)}$$

and its polarization referred to these axes is

$$P = \cos^2 \theta - \sin^2 \theta$$

The electric field E_p along the polaroid axis (at an angle ωt to the x-axis) is

$$E_p = A_0 \cos(\omega t - \theta) e^{i(kz-vt)}$$

The light then falls on a $\lambda/4$ plate with its fast axis at $\pi/4$ to the x-axis and its plane perpendicular to the z-axis calling E_{\parallel} the electric field along its fast axis and E_{\perp} the electric field along its retarding axis:

$$E_{\parallel} = E_p \cos(\pi/4 - \omega t) e^{i(kz-vt)}$$

$$E_{\perp} = E_p \cos(3\pi/4 - \omega t) e^{i(kz-vt)}$$

passing through the $\lambda/4$ plate E_{\parallel} suffers a phase shift δ and E_{\perp} suffers a phase shift $\delta + \pi/4$.

The components of the field after passing through the $\lambda/4$ plate are then:

$$E'_{\parallel} = E_{\parallel} e^{i\delta}$$

$$E'_{\perp} = E_{\perp} e^{i(\delta + \pi/4)}$$

or in terms of the x and y components:

$$E'_x = \frac{1}{\sqrt{2}}(E'_{\parallel} - E'_{\perp}) = \frac{1}{\sqrt{2}}(E_{\parallel} - iE_{\perp})$$

$$E'_y = \frac{1}{\sqrt{2}}(E'_u + E'_\perp) = \frac{1}{\sqrt{2}}(E_u + iE_\perp)$$

The monochromator passes $\alpha E'_y + \beta E'_x$ where its polarization = $\frac{\alpha^2 - \beta^2}{\alpha^2 + \beta^2}$ along the y-axis. The intensity of light appearing at the exit slit is then:

$$\begin{aligned} I &\propto (\alpha E'_y)^2 + (\beta E'_x)^2 \\ &= \frac{\alpha^2 + \beta^2}{2} (E^2 + E^2) \\ &= \frac{\alpha^2 + \beta^2}{2} E_p^2 \\ &= \frac{\alpha^2 + \beta^2}{2} \cos^2(\omega t - \theta) \end{aligned} \tag{11}$$

Thus we obtain a signal of exactly the same form we would have obtained if the monochromator were not there, reduced only by the factor $\frac{\alpha^2 + \beta^2}{2}$. The photomultiplier then produces a signal $V(t) = C \cdot \cos^2(\omega t - \theta)$ where C is a constant depending on the photomultiplier efficiency and gain, the efficiency of the optics, and the intensity of radiation emitted from the discharge.

§3.4 The Vacuum System

The vacuum system is shown in FIG. 10. It is a conventional glass system pumped by a "Cenco-Hyvac" mechanical pump which is capable of reducing the pressure in the system to less than 5×10^{-4} mm Hg when the liquid nitrogen cold trap to prevent backstreaming of pump oil is in place. Hydrogen gas is leaked into the system by a needle valve; the leakage rate establishing the equilibrium pressure of the system. When the discharge was submersed

in liquid nitrogen any impurities in the hydrogen tend to freeze on the walls of the discharge cell. The hydrogen obtained from a high pressure bottle is sufficiently impure that within a few hours the discharge cell walls become quite opaque, therefore two cold traps were installed further upstream.

Starting from the reduction valve on the pressure bottle, hydrogen at ~2 pounds/in² above atmospheric pressure passes through a flexible rubber hose to a cold trap filled halfway with activated charcoal. From the charcoal trap it proceeds through ~20 cm of hose to the needle valve and from there at low pressure to a second cold trap. Proceeding downstream from the second cold trap to the discharge cell, about halfway along, a Pirani and a McLeod gauge are attached to the system and connected via glass stopcocks. Proceeding downstream from the discharge cell another cold trap is encountered before the gas is pumped out by the mechanical pump. All the connecting glass tubing has an inside diameter of ~7 mm. Some flexibility in the position of the discharge cell was provided by the ground glass swivel joints by which it was attached to the vacuum system.

When data was being taken the pressure in the system was measured at about 2 hour intervals with the McLeod gauge and continuously monitored with the roughly calibrated Pirani gauge.

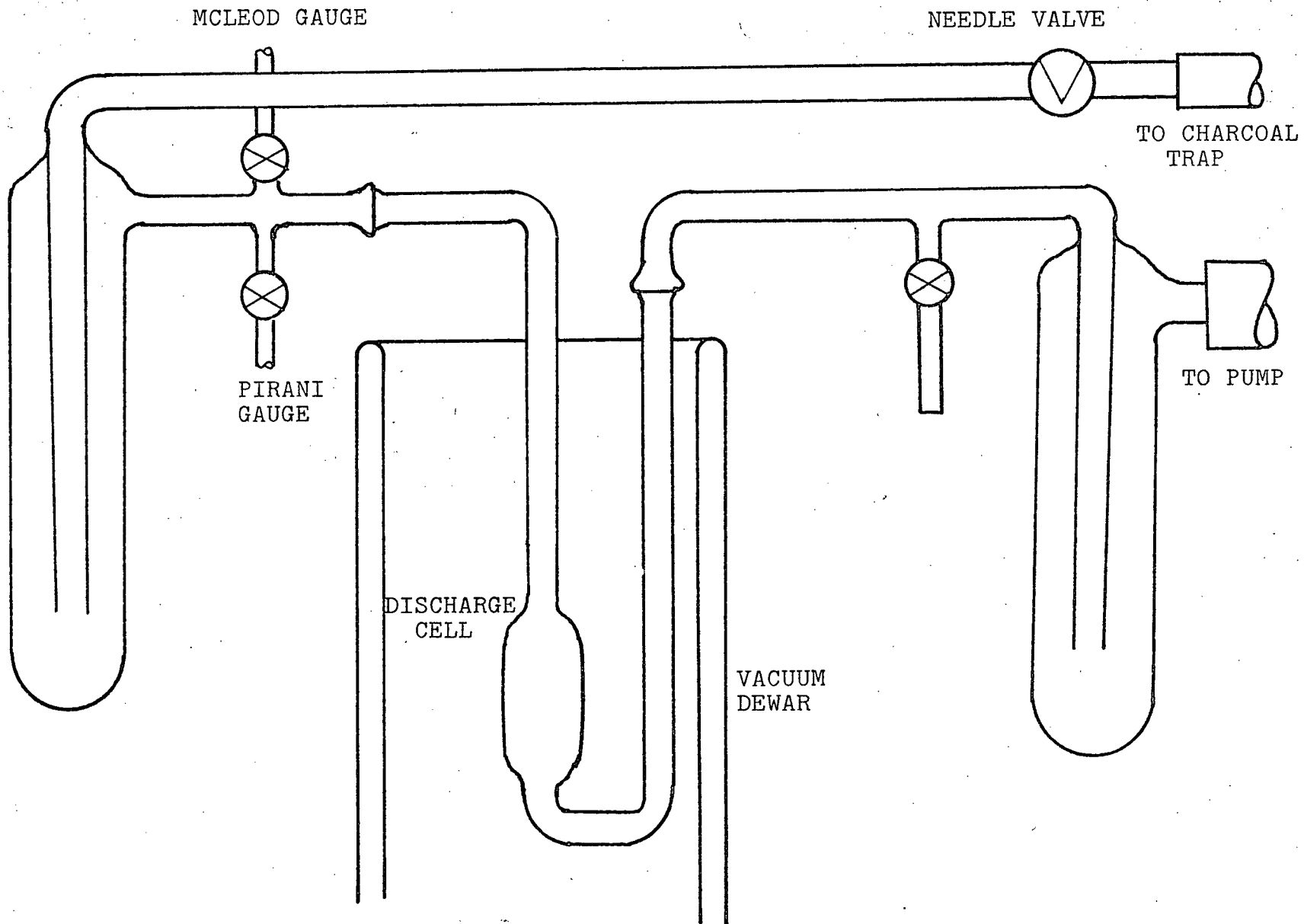


Figure 10 - The Vacuum System

§ 3.5 R.F. Supplies and Coupling

The 180 MHz source was a simple oscillator using a 928 B tube. Its schematic is shown in FIG. 11. The plates take on an R.F. voltage about ground potential while the cathode is fed from the negative terminal of a power supply at a potential of -80V to -600V. The "tank" circuit for the plates consists of a strip of thin copper sheet approximately 1 cm wide and 30 cm long, grounded at the centre and attached to one anode at either end. Feedback to the grids is provided by a 30 cm length of 16 gauge insulated copper wire whose loop is laid between the plate strip loop. At the plates the impedance and R.F. voltage is sufficiently high to obviate transformers or special coupling circuits. The discharge capacitor plates were coupled to the plate "tank" circuit by a length of 300Ω (characteristic impedance) twin lead wire. The wire was attached to the copper strip at points, equidistant from the grounded point, where maximum power transfer was estimated to occur. In practice, the maximum power transfer occurred at contact points about 8 cm from the centre.

The power output was estimated to be about 5 - 10W at a cathode potential of 300V. This oscillator had several drawbacks. The power output was quite unstable over periods exceeding 10 minutes, rather large fractions of R.F. power were radiated into the surrounding room, and the oscillator had a tendency to pulse its output in bursts repeated at intervals of order of 10^{-6} seconds.

TUBE = 928B

PHYSICAL CONSTRUCTION OF
DOTTED SECTION

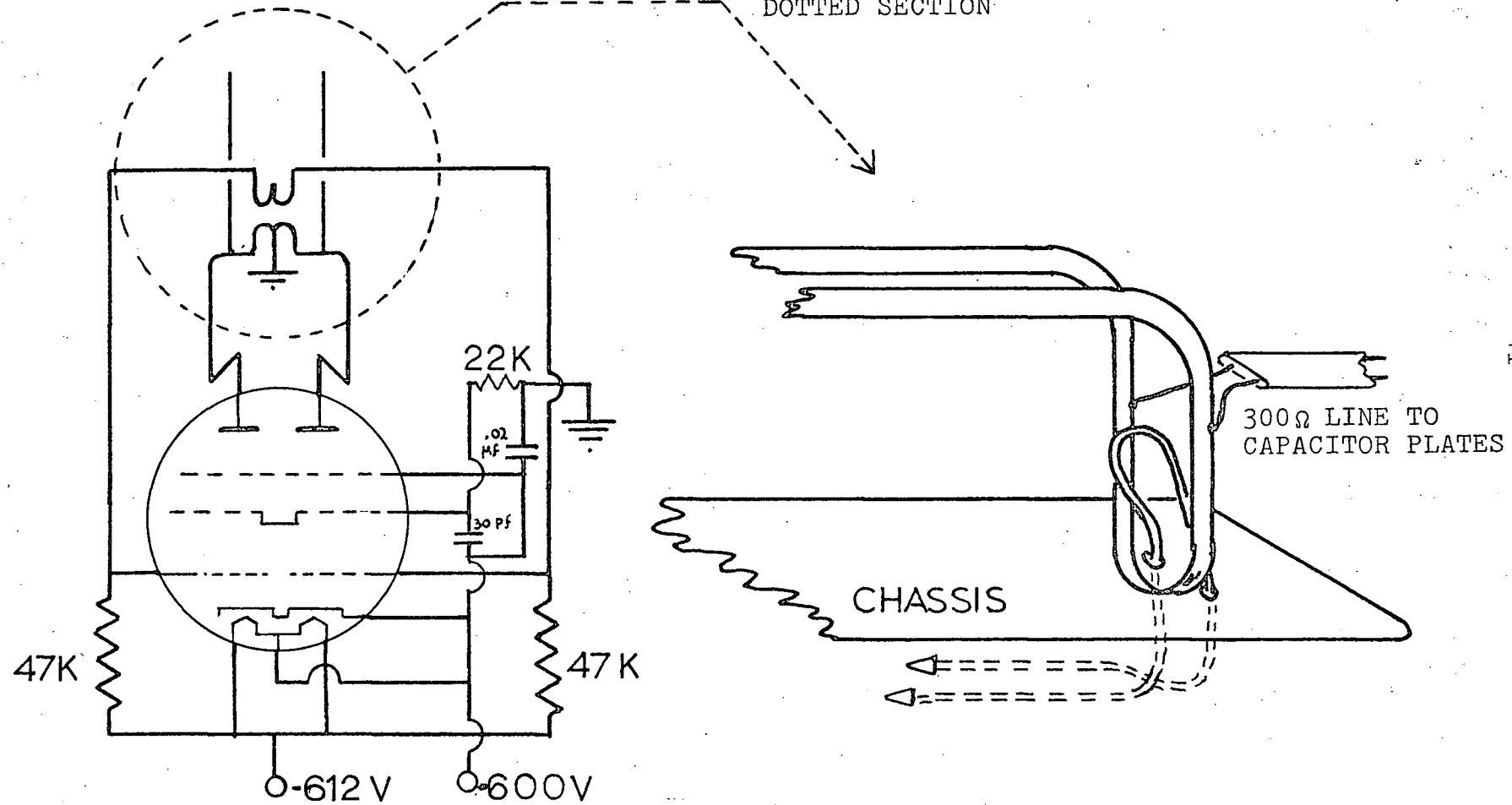


Figure 11 - 180 MHz R.F. Oscillator

Later, the source was replaced by a 450 MHz transmitter consisting of an R.C.A. MI-17436-1 transmitter used as "driver" and a Canadian Marconi Model 163-107 high frequency power amplifier with an output impedance of 50Ω and output power of approximately 50W. If we have a 1:1 standing wave ratio (S.W.R.) on a 50Ω line and 50W is transmitted, the R.F. voltage available is only 50V. Since we need a field of order 400V/cm between the discharge capacitor plates and the plates are spaced at 3 cm, 1200V is required. Voltages of this order were obtained by the "T matched" resonant circuit shown in FIG.12. A length of RG 8-U cable carried the power to this circuit. By adjustment of the contact point A (see FIG.12) an approximate impedance match between the resonant circuit and transmission line may be obtained. The circuit is tuned to resonance by moving the crossbars closer together or further apart, while keeping them equidistant from the capacitor plates.

§3.6 Helmholtz Coils

The earth's magnetic field cancelling coils have a 19.5 cm mean diameter, and are spaced 9.7 cm apart; each has 50 turns of #24 copper wire. When the 2 coils are placed in series the field produced at the centre is approximately 5 gauss/A. These coils are expected to reduce the earth's field to less than .01 gauss; i.e. by at least a factor of 50. The inhomogeneities near the centre are of

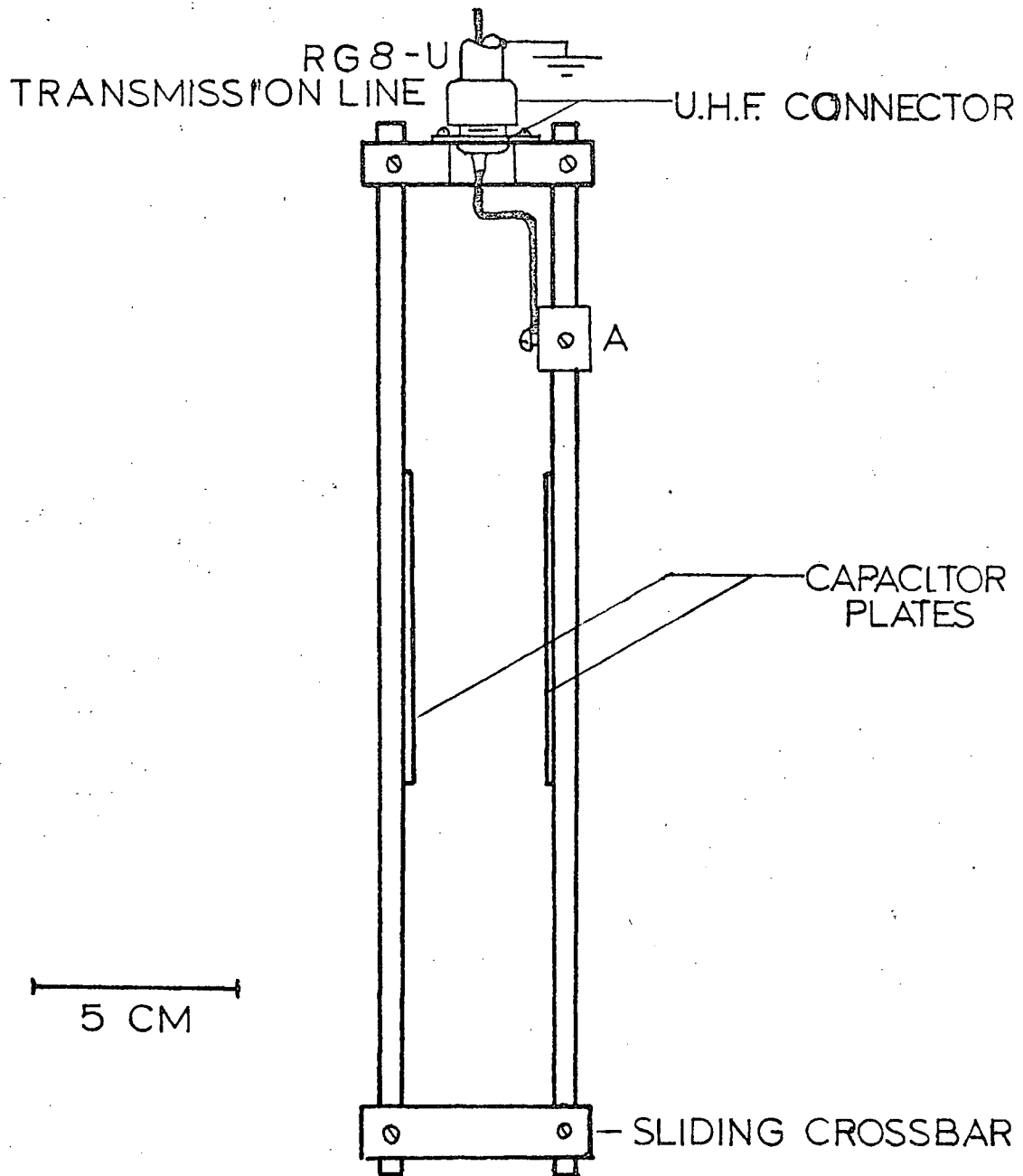


Figure 12 - R-Matched Resonant Circuit

order $(\frac{r}{R})^4$ where r is the displacement from the centre and R is the coil radius. For our 5 cm discharge cell, $(\frac{r}{R})^4 \sim (\frac{1}{4})^4$ or about 1 part per 250.

The coils which provide the applied magnetic field must have the same absolute homogeneity but this time in a total field of 10 gauss; i.e. they must provide for inhomogeneities $< 10^{-3}$. Therefore larger coils with a diameter of 37 cm and spacing of 18.5 cm were used. The inhomogeneities incurred with these coils should be roughly one part in 4×10^3 over the discharge region. These coils each had 100 turns of #18 copper wire. The coils were used in parallel and in this configuration the field produced at the centre is approximately 2.4 gauss/ampère.

There was no need to calibrate the smaller coils as it is only necessary to adjust the current until a zero field was reached. The vertical component of the earth's field within the Helmholtz coils was zeroed using a rotating coil with its axis of rotation along the horizontal component of the earth's magnetic field. Fields down to approximately .01 gauss could be detected this way. It was later found that a dip needle can be used to this effect with about the same accuracy.

The larger Helmholtz coils were calibrated in terms of voltage across the coils as a function of field within. The field measurements were made first with a

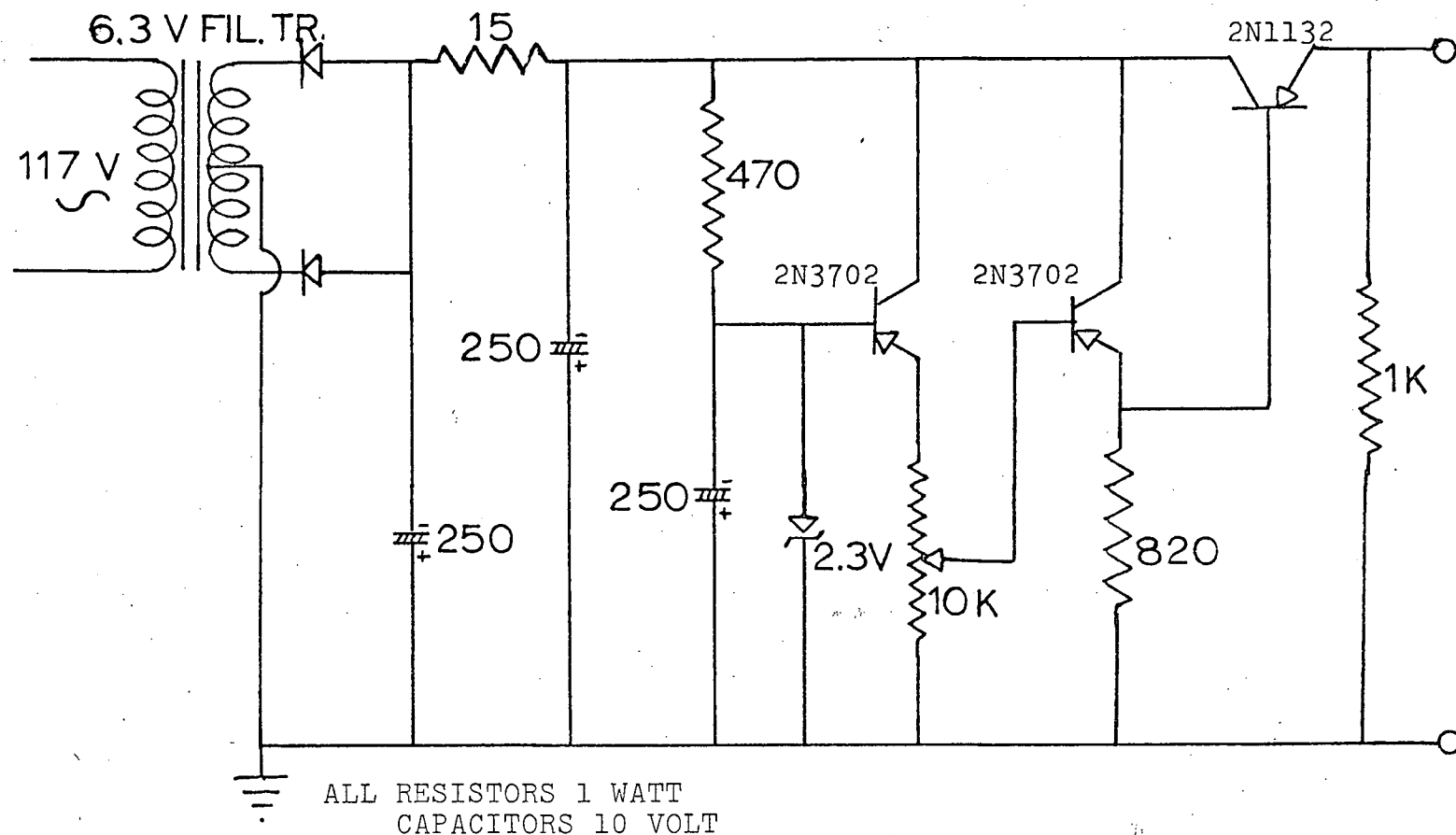


Figure 13 - Helmholtz Coil Power Supply

"Bell 240" Hall probe gaussmeter. Because of the somewhat erratic behavior of this gaussmeter the measurements were checked with a "Magnion FFC-4" rotating coil magnetometer. In order to save calibrating the x-channel of the x-y recorder, the position of the pen was measured as a function of field. With the recorder on the 2V/in scale (which was always used in its calibrated mode) the field in the discharge region was found to be $3.60 \pm .08$ gauss per inch of pen movement from the centre. The coils were usually run with a 1Ω resistor in series. The field produced was then $2.00 \pm .04$ gauss/in.

§3.7 Current Supplies for Helmholtz Coils

The current for the earth's field cancelling coils is provided by a small power supply delivering up to 1V and 150mA into the coils. Its schematic is shown in FIG.13. At 0.65V (~110mA) the ripple is approximately 1mV and the D.C. drift is less than 10mV.

The current delivered to the larger Helmholtz coils is supplied by a pair of "EICO 1064" power supplies and regulated by a D.C. power amplifier²⁸ whose schematic is shown in FIG.14. The amplifier delivers up to 7A of either polarity into a 1Ω load with reasonable linearity; has a voltage gain of approximately unity and an input impedance of approximately $10K\Omega$. The amplifier is controlled by the voltage supplied by a mechanically swept -10V to

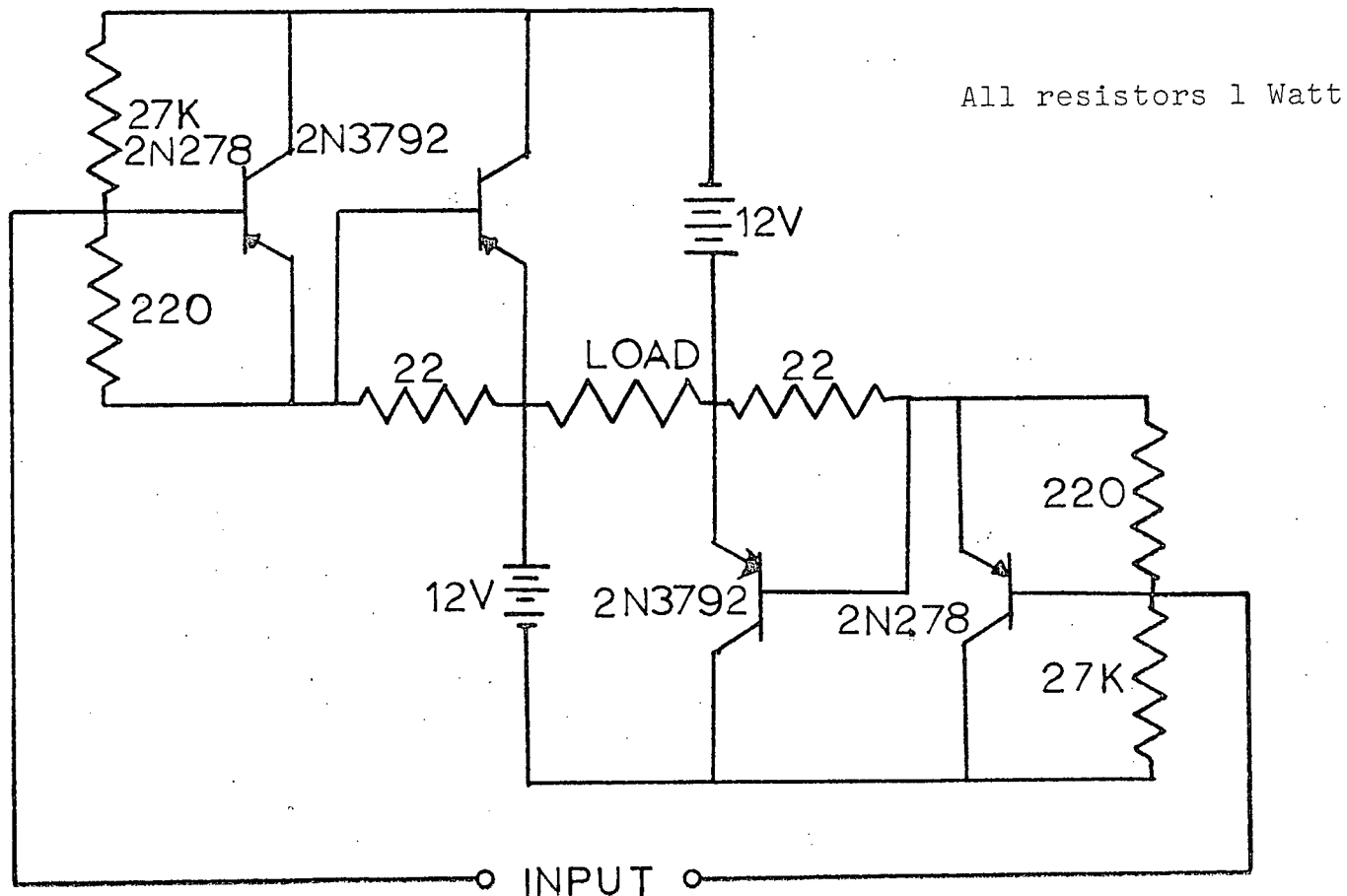


Figure 14 = D.C. Power Amplifier

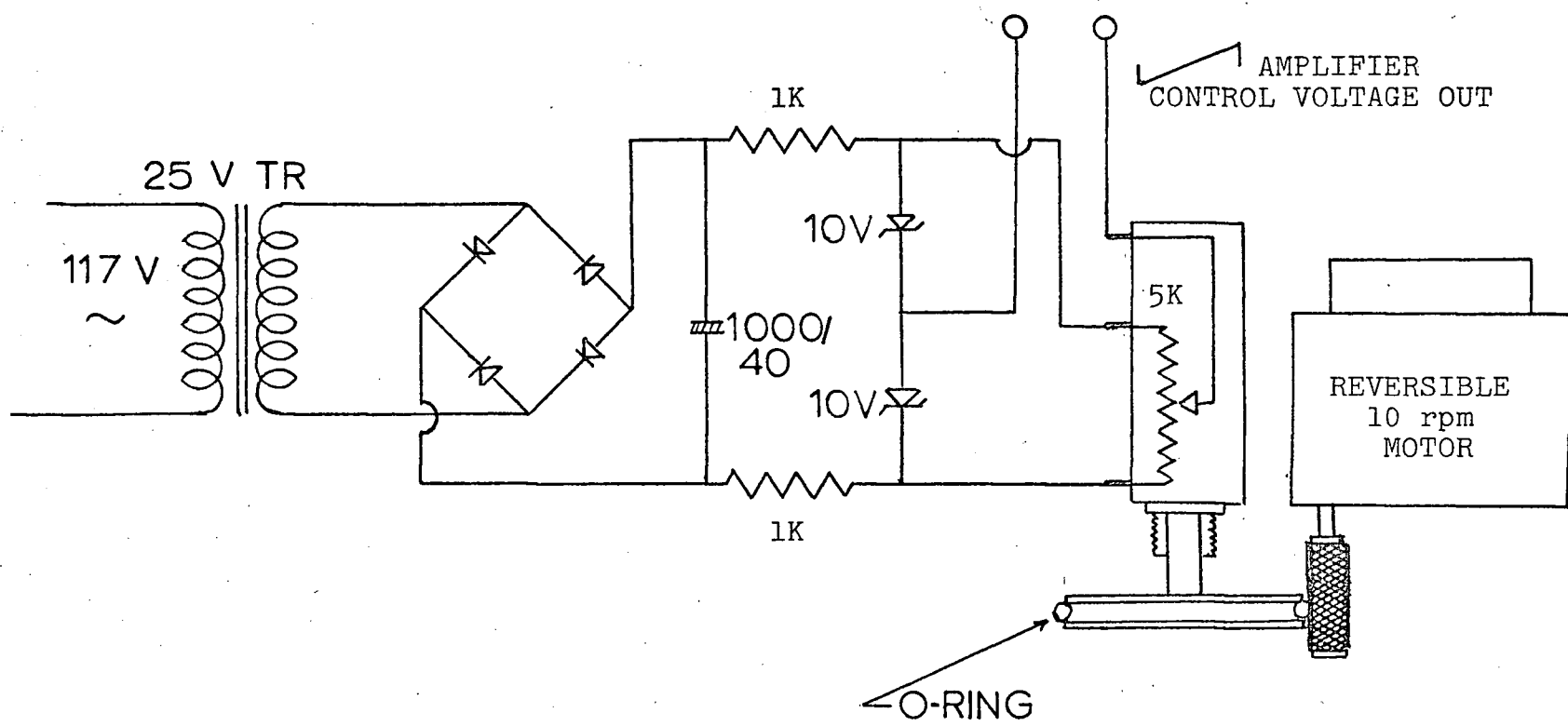


Figure 15 - -10V to +10V Voltage Sweep Mechanism

+10V source shown in FIG.15. The sweep time is about 7 minutes.

§3.8 Lock-in Amplifier

The lock-in amplifier consists of a tuned pre-amplifier with a Q of about 10 and a phase sensitive detector. The lock-in amplifier used in this experiment, Princeton Applied Research Model 120, has a linearity of 1% and a gain of 10^4 . The output is D.C. $\pm 10V$ at full scale. In the mode it was used, it supplies its own sinusoidal reference signal triggered by an externally supplied reference signal. In this experiment a 3 second time constant was used throughout.

The function of the phase sensitive detector is easily understood. Essentially, if given an input signal $V(t)$ it produces a signal

$$S \propto \frac{2\pi v}{\tau} \sum_{n=0}^{\tau/2\pi v} \int_{2n\pi}^{2(n+1)\pi} V(t) \cos(vt-\phi) d(vt)$$

where ϕ is a selected phase angle, v is the tuned frequency, and τ is the time constant. So long as τ is sufficiently large, incoherent signals will average to zero.

We can now see what the lock-in amplifier does to our signal derived in eq.(11) § 3.3.

$$S \propto \int_0^{2\pi} \cos^2(\omega t-\theta) \cos(vt-\phi) d(vt)$$

Choosing $v=2\omega$ and $\phi=0$,

$$S \propto \int_0^{2\pi} \cos^2(\omega t - \theta) \cos 2\omega t \, d(2\omega t)$$

$$\propto \cos 2\theta = \cos^2 \theta - \sin^2 \theta = P$$

In other words, the lock-in amplifier output signal is just proportional to the polarization of the emitted light referred to the x-axis.

§3.9 The Rotating Polaroid

The polaroid rotator is shown in FIG.16. The polaroid is glued to a 2" I.D. brass pipe which is fitted tightly inside a large ball-bearing. A sewing machine belt laid over the pipe and the motor pulley rotates the polaroid. The motor, model CA3GRH, Universal Electric Co., runs at 1050 r.p.m. and delivers $\frac{1}{20}$ H.P. The motor pulley has a 2" diameter and a belt groove of $1\frac{11}{16}$ inch diameter. With this arrangement the polaroid is rotated at approximately 14 cycles/second.

The light to be "chopped" passes through the centre of the pipe. Two quarter segments of the rim of the polaroid are painted black to interrupt light from a small lamp behind the polaroid periodically as the polaroid turns. Light from the lamp falls on a photodiode, placed in front of the polaroid disk.

§3.10 The Variable Quarter-Wave Plate

The quarter-wave plate used is based on one described by Happer and Saloman²⁹.

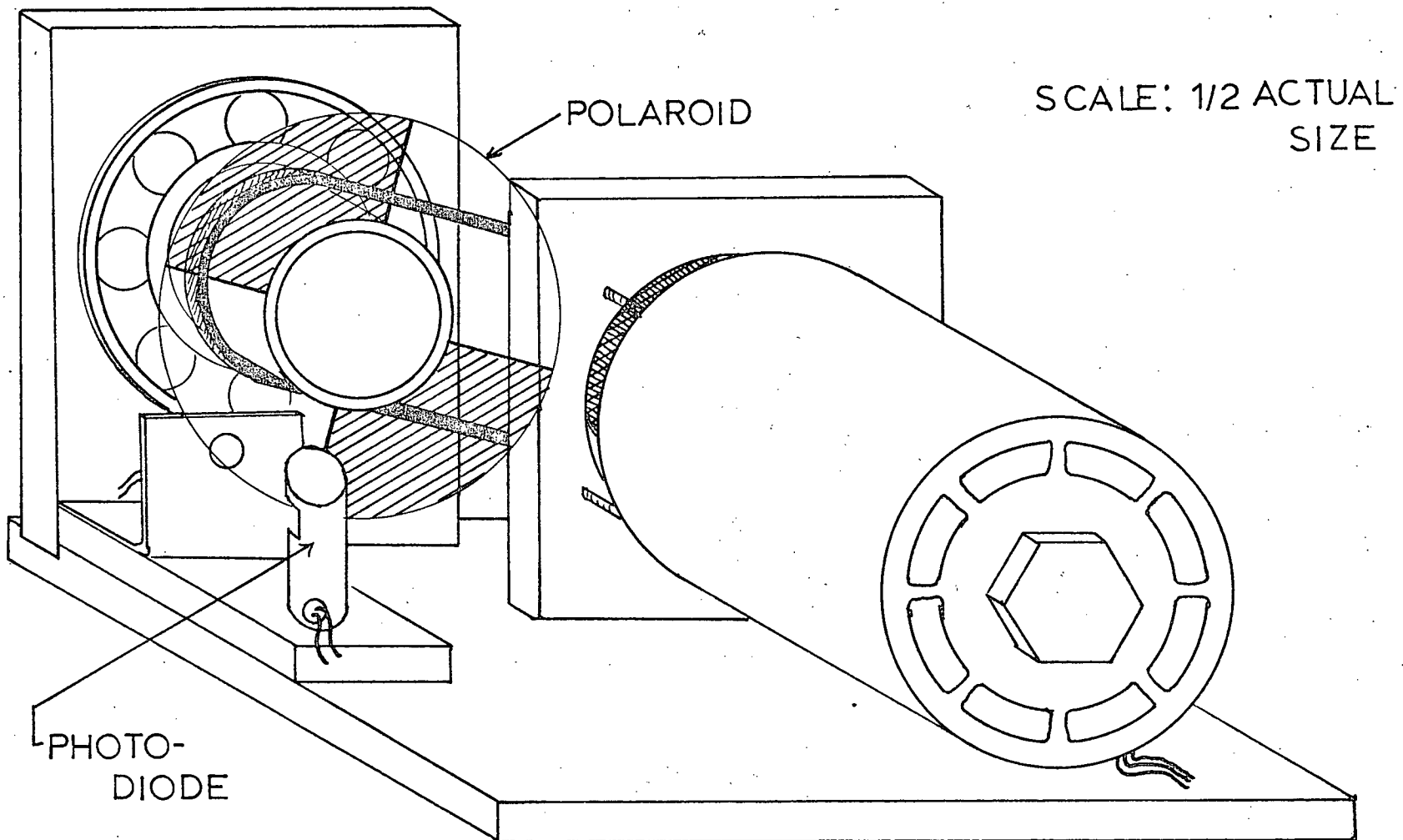
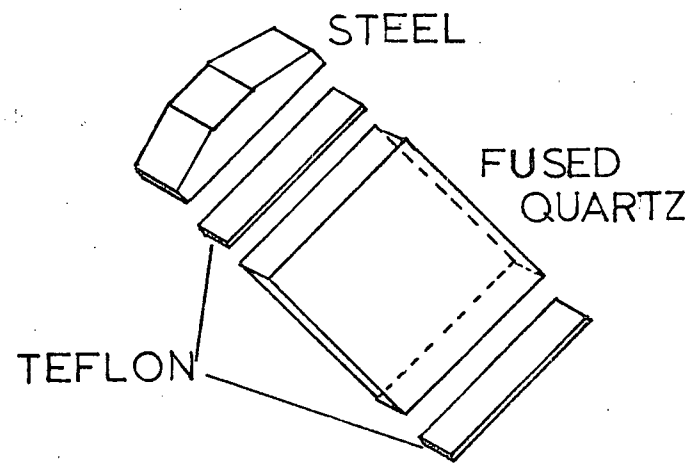
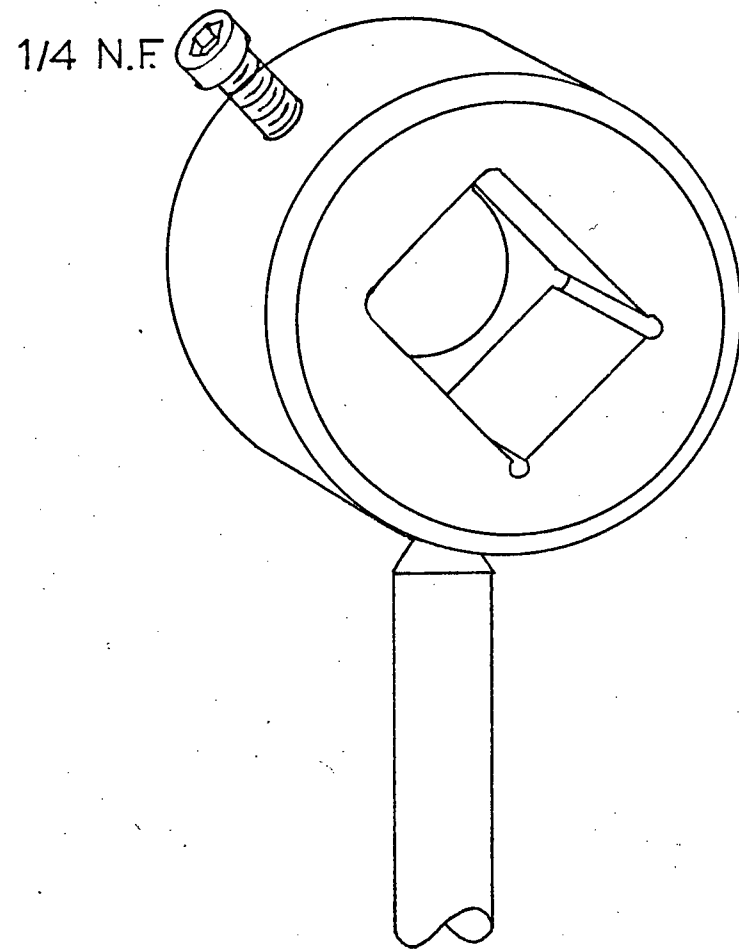


Figure 16 - Polaroid Rotator

When fused quartz is stressed it becomes birefringent with its optical axis along the direction of strain. The relative retardation between a wave with electric vector parallel - and one with its electric vector perpendicular to the direction of strain increases with the stress applied. This effect is made use of to construct the variable wavelength quarter-wave plate shown in FIG.17.

The major components are a piece of fused quartz $1" \times 1" \times \frac{3}{16}"$ ground flat and parallel on two opposing edges, a brass case, and a steel pressure plate to distribute the force from a $\frac{1}{4}"$ N.F. thread screw over the ground face of the quartz plate. In an effort to reduce the pressure inhomogeneities due to irregularities of the contact surfaces; the surfaces of the steel plate, the quartz plate, and the inside bottom surface of the case are spaced by 2 pieces of $\frac{1}{16}" \times \frac{3}{8}" \times 1"$ teflon. Eye inspection with crossed polaroids while the screw is tightened to strain the quartz shows that except at the corners a fairly homogeneous quarter-wave plate is produced.

The quarter-wave plate is adjusted by tightening the screw until unpolarized light from the discharge produces a zero output signal from the lock-in amplifier.



FULL SCALE

Figure 17 - Quarter-Wave Plate

§3.11 Photomultiplier

The photomultiplier used for this experiment is an E.M.I. 9558QB. It has an S-20 (NaKSbCs) surface. The quantum efficiency at 4900 \AA is said by the manufacturer to be ~23%. It was operated with a cathode to anode potential of -1280V. The dynode chain resistors were all $33\text{K}\Omega$ while the cathode to first dynode potential is maintained at -150V by a zener diode. The anode is connected to ground by a $100\text{K}\Omega$ resistor. The abbreviated circuit is shown below in FIG.18.

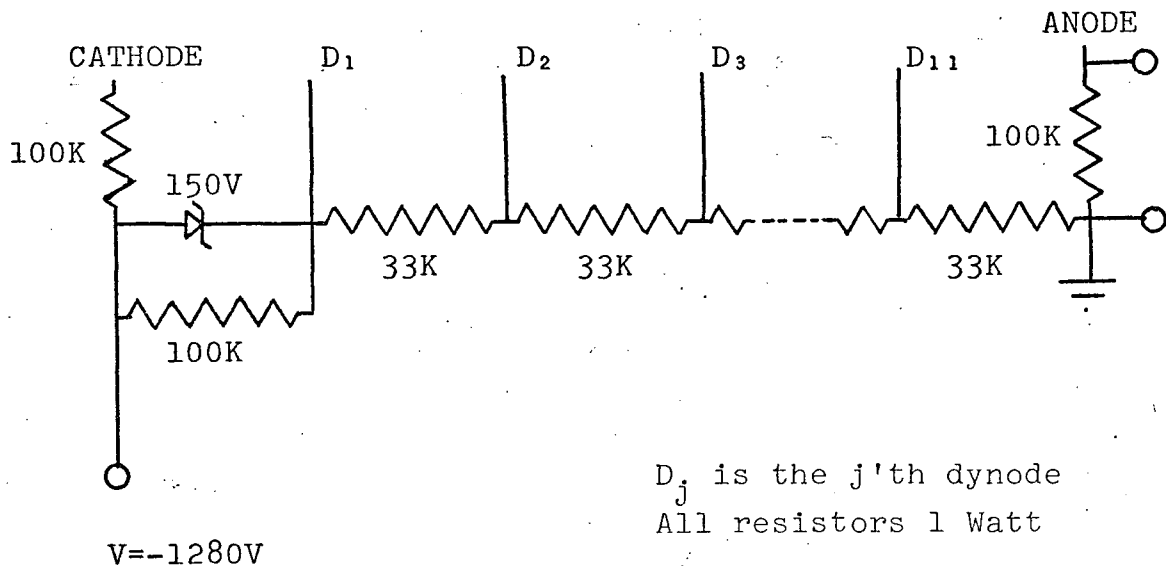


Figure 18 - Photomultiplier Wiring Schematic

§3.12 X-Y Recorder

The x-y recorder used was a Varian model F100 having a linearity of 1% and input impedance of $100\text{K}\Omega$ into each channel.

§3.13 Liquid Nitrogen Bath

The R(0), R(1), and R(2) lines of the (0,0) band of the $3d^1\Sigma \rightarrow 2p^1\Pi$ transition are separated by about 3\AA which is easily resolved by the monochromator with fairly wide slits. The R(4) line of the same electronic, vibrational transition however falls almost on the R(1) line and has about the same intensity. It was found that cooling the discharge eliminated the line almost completely. This is not surprising since the R(4) transition arises from the $J' = 5$ level of the upper state. Under the selection rule derived in the theory section this level is populated from the $J = 3$ level of the ground state. Thus the line strength of R(4) would be expected to be proportional to the population of the ground state $J = 3$ level. Referring to Table I, §2.4, we see that whereas $J = 3$ has an appreciable population at room temperature (compared with the $J = 0$ and $J = 2$ from which R(1) arises), at liquid nitrogen temperatures its population is negligible. To lower the temperature of the discharge, the discharge cell is placed inside a large vacuum Dewar fitted with a 2 inch diameter flat window on the front outside side, and the Dewar is filled with liquid nitrogen. The liquid nitrogen level decreased at a rate of roughly $\frac{1}{2}$ inch per hour and was observed to boil at the surface of the discharge cell only when the H_2 pressure inside exceeded 200μ .

§3.14 Data Processing

The graphs plotted by the x-y recorder (see FIGs.19 and 21) were subjected to numerical processing to extract the halfwidth, $H_{1/2}$. Relative values of the polarization were read from the graphs at 0.2 inch intervals to provide 39 data points. The points were then used to fit a function of the form:

$$P = C_1 + \frac{C_2}{1 + \frac{1}{H_{1/2}^2} (H - H_o)^2} [\cos 2\theta - \frac{1}{H_{1/2}} (H - H_o) \sin 2\theta] \quad (12)$$

where C_1 , C_2 , $H_{1/2}$, H_o and θ are parameters fitted by a computer "least squares" fitting routine (U.B.C. L.Q.F.). The fitted curves are shown in FIGs.20 and 22. At each of the hydrogen pressures used, 6 to 8 (depending on signal to noise) graphs were produced and independently fitted by (12). The average $H_{1/2}$ was then computed for that pressure, plotted as a function of pressure and extrapolated to zero pressure (see FIGs.23 and 24). From these $H_{1/2}$ v.s. pressure graphs the radiative lifetime and cross-sections are computed as will be seen in the next chapter.

CHAPTER IV

EXPERIMENTAL RESULTS

§ 4.1 Lifetimes

A typical experimental plot of the polarization curve obtained, using the 450 MHz discharge, is shown in FIG.19. A similar graph is shown in FIG.21 for the discharge excited by the 180 MHz R.F. field. Their respective "least squares" fitted curves are shown in FIG.20 and 22. The polarization scale is arbitrary and normalized to 0.9 on the computer generated plots. The halfwidths of the curves obtained at the various pressures are tabulated in Table III.

In figures 23 and 24 the average halfwidths, $H_{1/2}$, of the curves are shown as a function of pressure in the vacuum system. The error bars in $H_{1/2}$ represent statistical errors only, while the error bars in pressure represent the maximum error in reading the McLeod guage.

The halfwidth of a line at zero pressure may be converted to the upper-state's lifetime, using:

$$\tau_J = \frac{1}{2g_J\mu_0 H_{1/2}}, \quad \mu_0 \text{ is the Bohr magneton.}$$

The extrapolated halfwidths and lifetimes levels of the $J=1, 2$, and 3 of the $3d^1\Sigma, v=0$ state are tabulated in table IV. The g factors used are those given by Dieke³⁰.

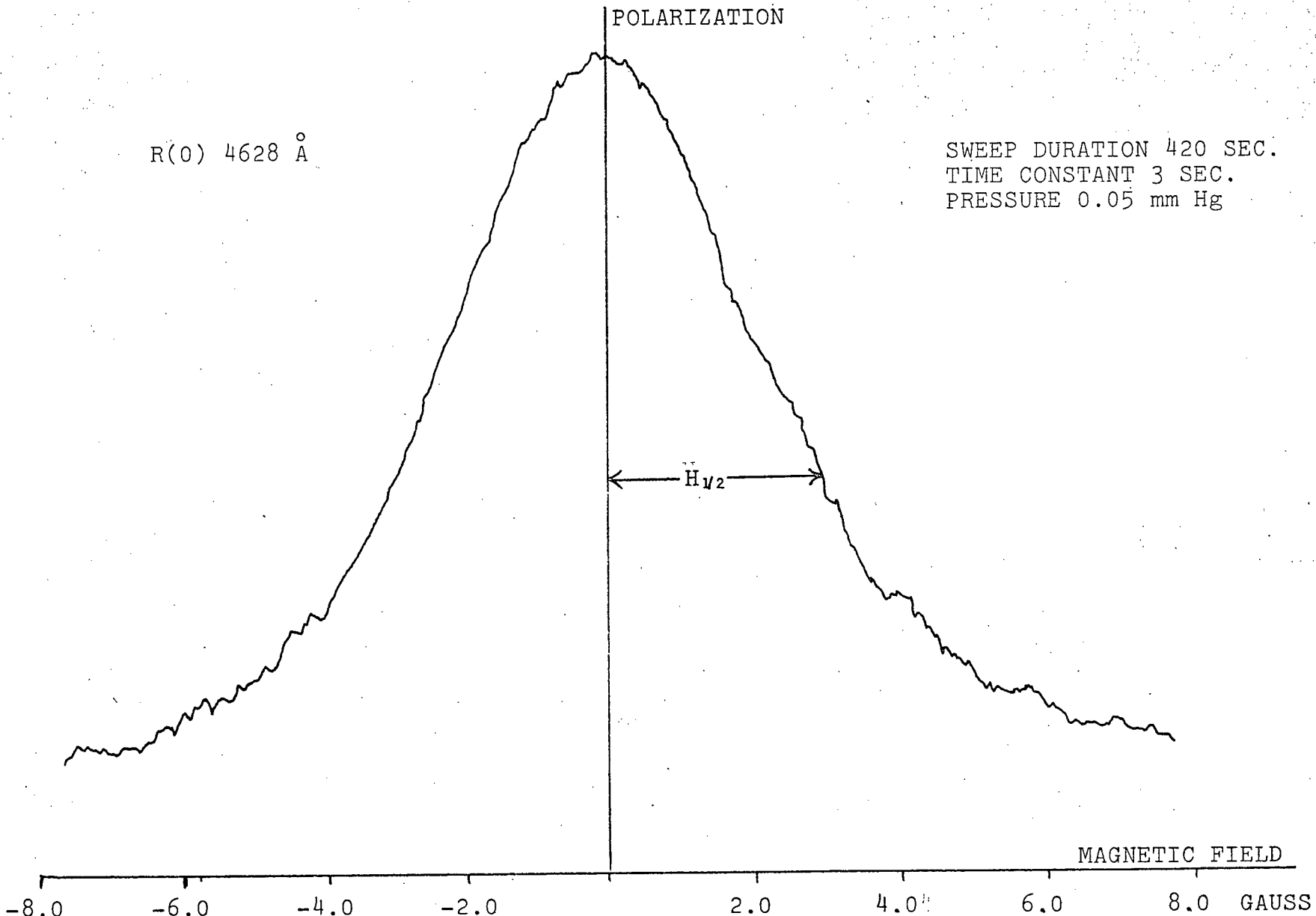


Figure 19 - Experimental Level-Crossing Curve for the R(0) Line
Using 450 MHz Excitation

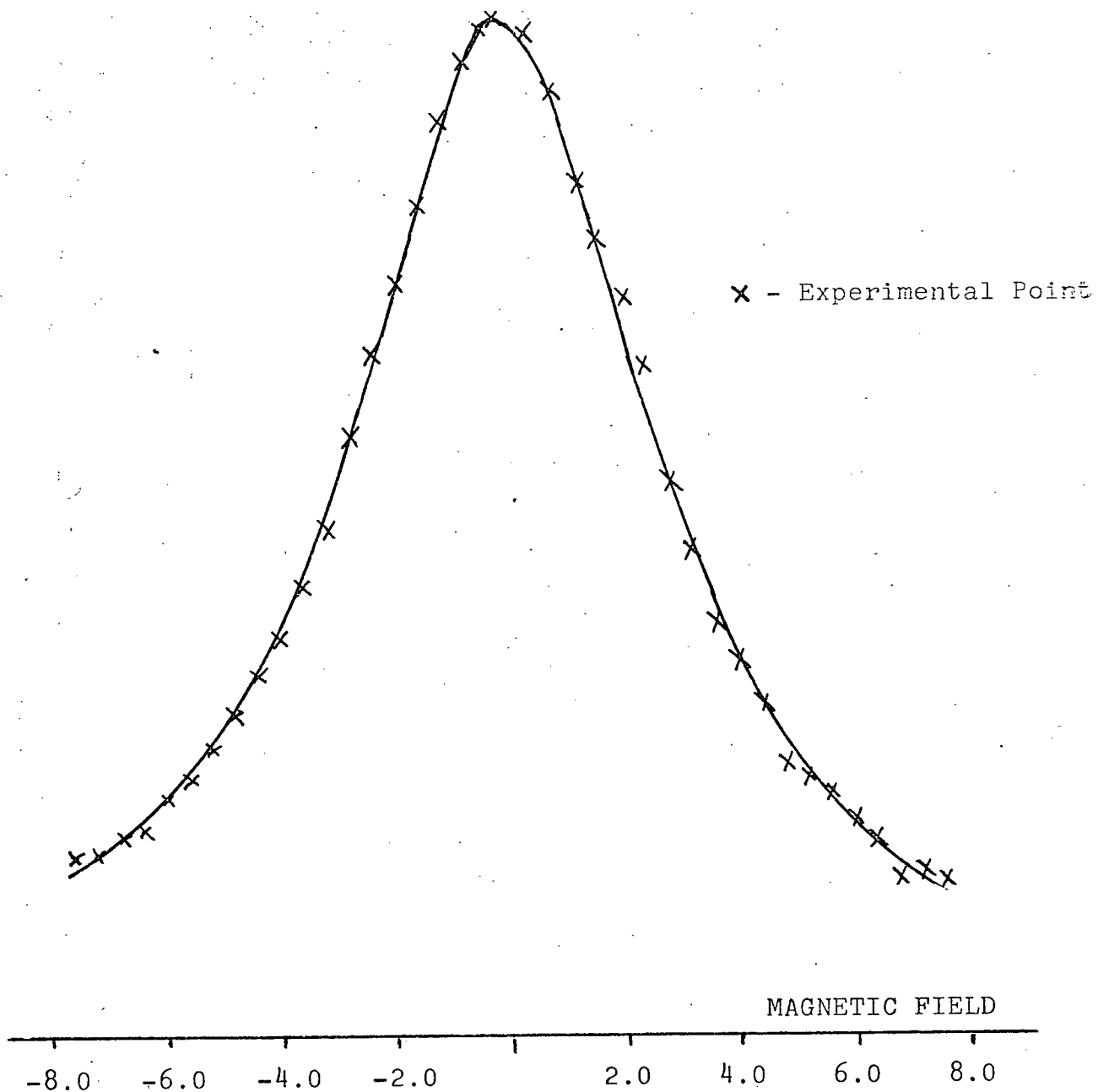


Figure 20 - Least Squares Fitted Curve for the R(0) Line Using 450 MHz Excitation

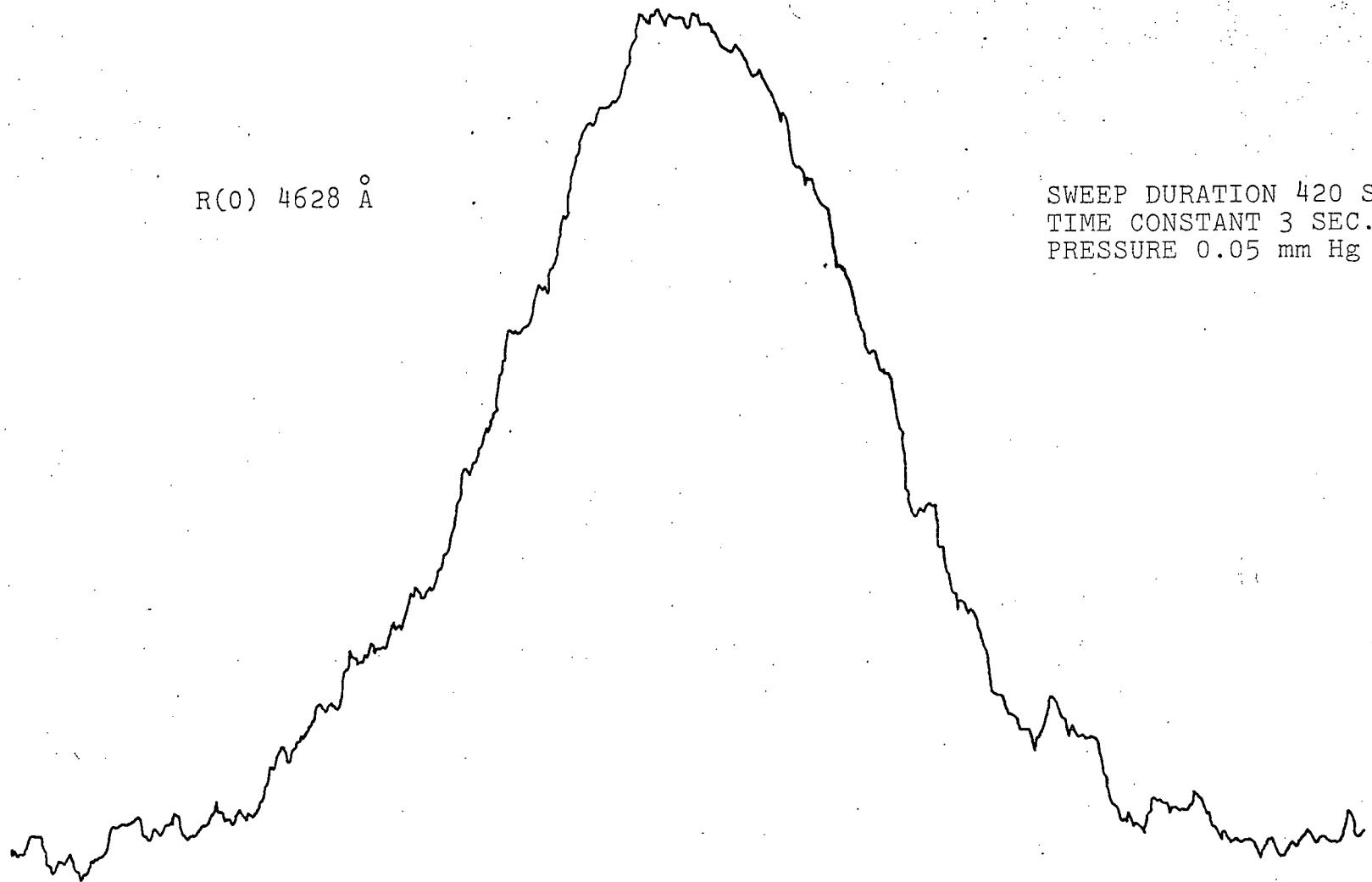


Figure 21 - Experimental Level-Crossing Curve for the R(0) Line
Using 180 MHz Excitation

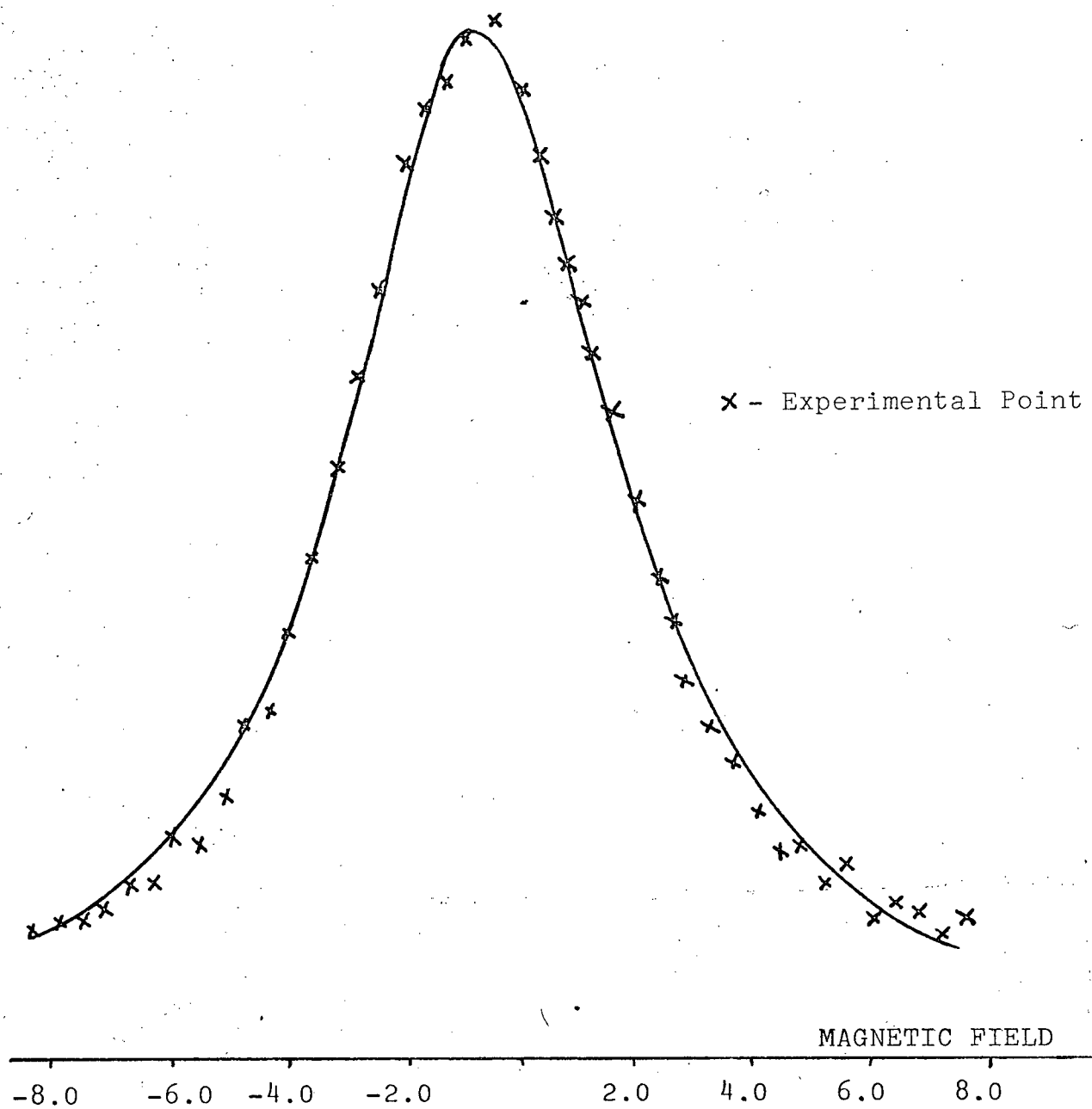


Figure 22 - Least Squares Fitted Curve for the R(0) Line Using 180 MHz Excitation

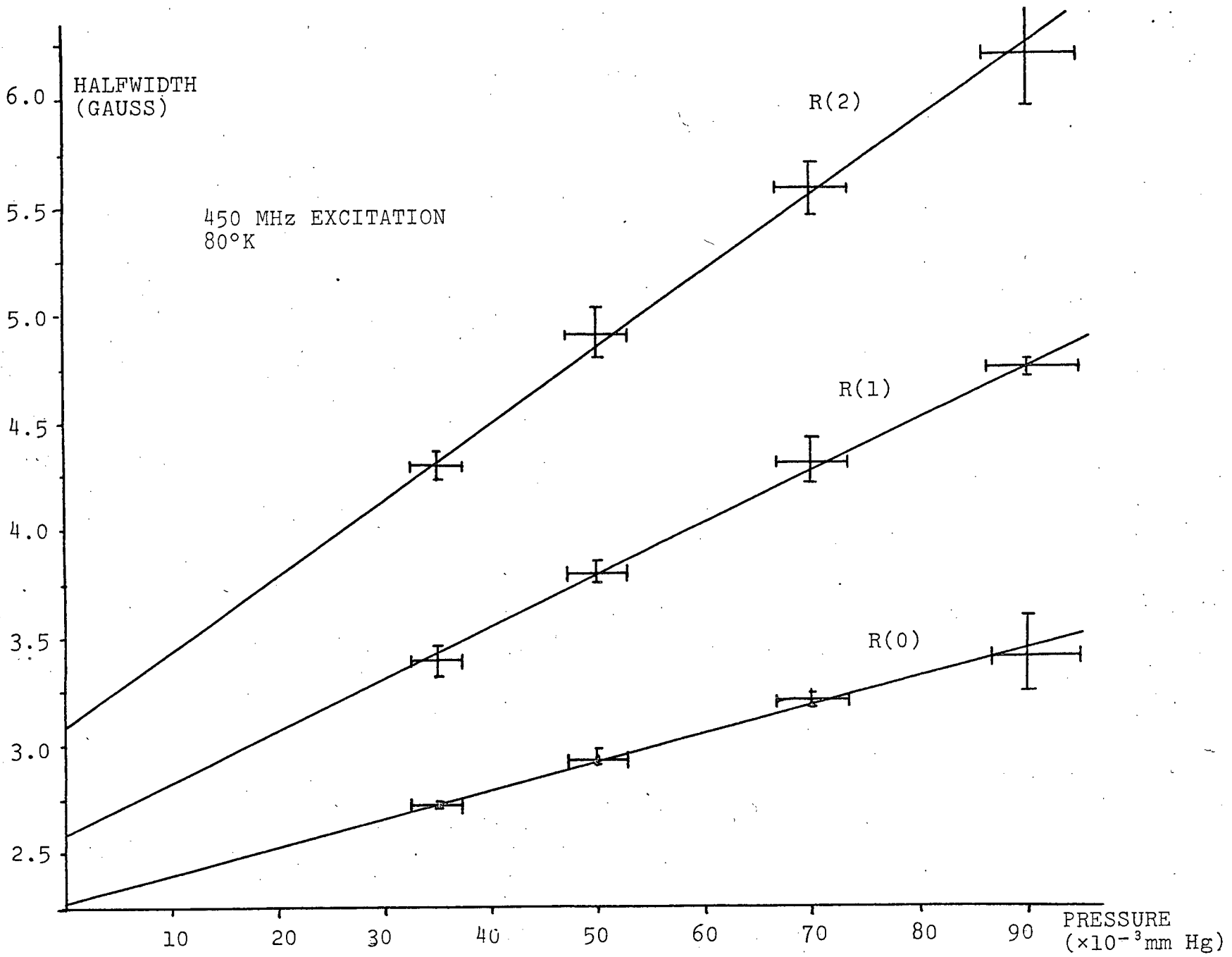


Figure 23. - Level Crossing Curve Halfwidth as a Function of Pressure

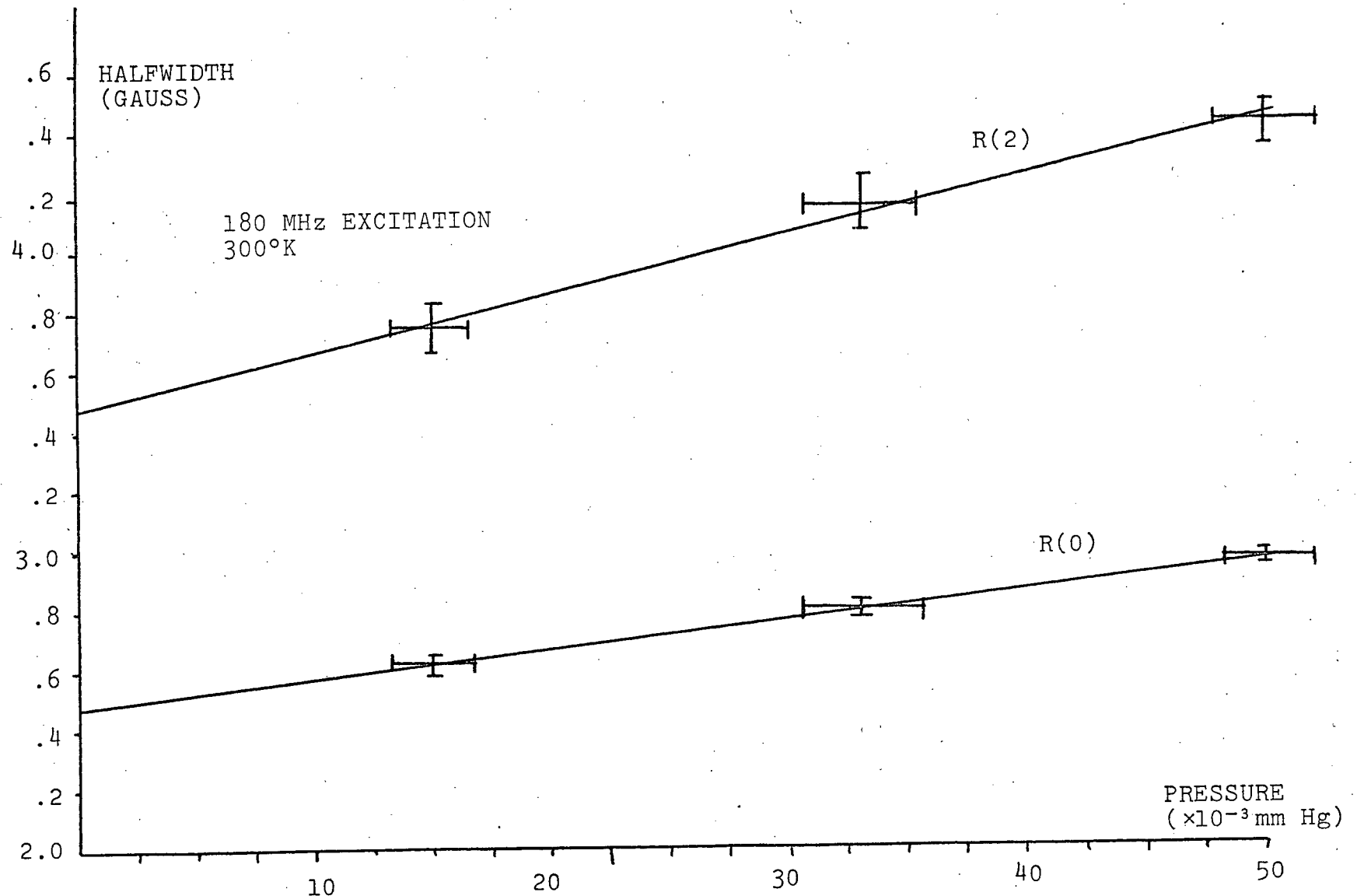


Figure 24 - Level Crossing Curve Halfwidth as a Function of Pressure

J	g_J	$H_{1/2}$ (gauss) 300°K 180MHz	$H_{1/2}$ (gauss) 80°K 450 MHz	$\tau(10^{-8} \text{ sec})$ 300°K 180MHz	$\tau(10^{-8} \text{ sec})$ 80°K 450MHz
1	.901	$2.47 \pm .1$	$2.27 \pm .1$	2.55	2.78
2	.571		$2.60 \pm .08$		3.83
3	.445	$3.41 \pm .1$	$3.10 \pm .2$	3.74	4.12

Table IV - Extrapolated Halfwidths and Lifetimes

The halfwidths obtained for each of the individual runs is contained in Table V.

§4.2 Collision Cross-sections

From the slope of the $H_{1/2}$ v.s. pressure graphs, a reasonable estimate of the collision cross-sections may be obtained if one makes some plausible assumptions about conditions in the discharge.

We assume that the number of free electrons in the discharge is small compared to the number of neutral molecules, and we assume that the number of excited molecules is small compared to the number of ground state molecules; then any collision an excited molecule suffers will be with one in the ground state. The equation for the upper state population, N^* , for molecules excited at time $t=0$, may then be written in terms of the two competing decay processes,

$$\frac{dN^*}{dt} = -\Gamma_0 N^* - \sigma v N^* N \quad (13)$$

R(0) 450 MHz

	90μ	70μ	50μ	35μ
	3.43194	3.14845	2.71100	2.75137
	3.40270	3.25614	3.17868	2.69689
	3.43443	3.15160	2.92867	2.74707
	3.48059	3.20694	2.98884	2.68692
		3.33747	3.02103	2.74468
		3.23944	2.82810	2.75787
average	<u>3.437±.18</u>	<u>3.223±.031</u>	<u>2.943±.07</u>	<u>2.731±.014</u>

R(1) 450 MHz

	4.61027	4.41363	3.93656	3.44569
	4.91537	4.26093	3.76604	3.41708
	4.62872	4.38411	3.74870	3.32601
	4.52513	4.39620	3.45032	3.38945
	4.84251	4.12871	4.00709	3.53151
	4.81395		3.96007	3.39896
average	<u>4.723±.07</u>	<u>4.317±.06</u>	<u>3.811±.09</u>	<u>3.418±.03</u>

R(2) 450 MHz

	6.10883	5.41178	5.18763	4.43328
	5.54281	5.91381	4.72888	4.54597
	6.97308	5.31858	4.94178	4.12689
	5.98210	5.85825	4.80084	4.17776
	6.74916	5.61430		4.26244
	5.86058	5.91132		4.34724
average	<u>6.203±.25</u>	<u>5.676±.13</u>	<u>4.915±.11</u>	<u>4.316±.07</u>

Table V - Polarization Curves' Halfwidths

R(0) 180 MHz

	15 μ	33 μ	50 μ
	2.60260	2.85038	2.96818
	2.87502	2.88300	3.03098
	2.51146	2.70572	2.90821
	2.64745	2.79014	2.95136
	2.57688	2.83666	2.98517
	2.67594		
average	2.648±.056	2.813±.035	2.969±.022

R(2) 180 MHz

	3.74852	4.33185	4.33183
	3.87775	4.08811	4.35565
	3.64140	4.12431	4.43897
	3.57200	4.22226	4.31595
	3.96459		4.65773
average	3.761±.1	4.192±.065	4.420±.07

Table V(continued) - Polarization Curves' Halfwidths

where Γ_0 is the radiative transition probability, σ is the collision cross-section, v is the relative velocity of colliding molecules, and N is the density of neutral molecules.

Solving eq.(13) we obtain

$$N^*(t) = N_0 e^{-\Gamma_0 t - \sigma v N t} = N_0 e^{-\Gamma(N)t}$$

thus the inverse lifetime

$$\frac{1}{\tau} = \Gamma(N) = \Gamma_0 + \sigma v N$$

then

$$\frac{d\Gamma}{dN} = \sigma v \quad \text{or,} \quad \sigma = \frac{d\Gamma/dN}{v} \quad (14)$$

from our graphs we have $\frac{dH_{1/2}}{dp}$, which may be related to $\frac{d\Gamma}{dN}$ by the following substitutions

$$\Gamma = 2g_J \mu_0 H$$

$$N \approx \frac{N_0 P T_0}{T}$$

where N_0 is Avogadro's number/Molar volume

P is the pressure in standard atmospheres

$$T_0 = 297^\circ K$$

T is the absolute temperature of the gas in $^\circ K$

then

$$\frac{d\Gamma}{dN} = \frac{2g_J \mu_0 T}{N_0 T_0} \frac{dH_{1/2}}{dp}$$

or more conveniently

$$\frac{d\Gamma}{dN} = 4.98 \times 10^{-7} \frac{\text{cm}^3 \mu}{\text{gauss sec}} \frac{T}{T_0} g_J \frac{dH_{1/2}}{dp}$$

finally, substituting this into eq.(14)

$$\sigma = 4.98 \times 10^{-7} \frac{Tg_J}{T_o V} \frac{dH_{1/2}}{dp} \frac{cm^3 \mu}{gauss sec}$$

where $H_{1/2}$ is measured in gauss and P is measured in microns
 $(= 10^{-3} mm Hg)$.

The values obtained for the collision cross-section, assuming $T = 300^\circ K$ in the room temperature discharge and $80^\circ K$ in the liquid nitrogen cooled discharge, and assuming Boltzmann velocities, are listed in Table VI. It is also assumed in calculating these cross-sections that the pressure in the discharge cell is that measured by the McLeod gauge.

J	σ $T=300^\circ K$	σ $T=80^\circ K$
1	$157 \text{ } \text{\AA}^2$	$102 \text{ } \text{\AA}^2$
2		$116 \text{ } \text{\AA}^2$
3	$167 \text{ } \text{\AA}^2$	$131 \text{ } \text{\AA}^2$

Table VI - Collision Cross-sections

§4.3 Polarization

The absolute polarization of the light observed at zero magnetic field was measured by placing a stationary polaroid in the light beam and comparing the lock-in amplifier output, S_0 , with that obtained without the second polaroid, S_1 . The polarization P of the light is then obtained from:

$$P = \frac{S_1}{2TS_0}, \text{ where } T \text{ is the polaroid transmittance.}$$

Under the best conditions, the polarizations thus found were at 20μ pressure of order 10%, 10%, and 5% for the R(0), R(1), and R(2) lines respectively. P varies widely with the conditions of the discharge. Qualitatively, the polarization decreases with increasing pressure, at 100μ it is roughly half of that observed at 50μ . Impurities in the discharge also decrease the polarization considerably.

§4.4 Upper State Populations

If the electronic-vibrational wave function of a molecule does not vary too drastically with increasing rotation, the relative populations of the rotational levels of the excited state may be computed from the relative intensity of transitions to the lower state. The relative population $N_{J'}$ of the state J' is then proportional to the sum of the intensities of the R, P, and Q transitions arising from the same upper state. Denoting the intensity of the transition A(J) (A represents R, P, or Q) by $I_{A(J)}$,

$$N_{J'} \propto I_{R(J'-1)} + I_{Q(J')} + I_{P(J'+1)}$$

Assuming a constant spectral response of the photomultiplier and constant monochromator efficiency over the $\sim 100\text{\AA}$ scanned, the relative intensities of the relevant transitions were measured to $\sim 10\%$ accuracy and the populations $N_{J'}$, computed. Q(J) is completely absent from the $\Sigma \rightarrow \Sigma$ bands hence the sum reduces to:

$$N_{J'} \propto I_{R(J'-1)} + I_{P(J'+1)}$$

The numbers $N_{J'}$, experimentally obtained normalized so that their sum equals unity are listed in Table VII. The numbers in the column headed by 300°K pertain to the discharge at room temperature while those headed by 80°K pertain to the discharge immersed in liquid nitrogen. Comparing these populations to those of the ground state given in Table I (§2.4) suggests that the selection rule $\Delta J=0, \pm 2$ derived in chapter II is fairly well obeyed.

J	$N_{J'}$ 325°K	$N_{J'}$ 80°K
0	.017*	.007*
1	.241	.281
2	.128	.193
3	.358	.406
4	.072*	.031*
5	.127	.052

Table VII - Experimental Upper State Populations

* P(1) and R(3) can not be resolved by our apparatus. The values given assume that $J'=4$ has at least half the population of $J'=5$. Probably the population of $J'=0$ is less than that stated, while the population of $J'=4$ is greater.

§4.5 Experimental Errors

a) Discharge Stability

The most serious experimental shortcoming is the sensitivity of the discharge to the magnetic field applied. An up to 10% decrease in intensity could be observed at fields of about ± 15 gauss. The effect was not reproducible enough to permit any gain in taking account of it in the curve fittings. As might be expected the effect was worst at the lowest pressures, where the discharge was somewhat unstable even without any magnetic field.

Assuming that the intensity of light emitted varies as $I_o(1-C^2H^2)$ with $C \sim O(10^{-2} \text{ gauss}^{-1})$, the apparent polarization curve then produced is of the form

$$(1-C^2H^2) \frac{1}{1+(2\mu H\tau)^2}$$

and for -10 gauss $\leq H \leq +10$ gauss the Lorentzian fitted has a halfwidth only a fraction of a percent smaller than that without the factor. The optical surfaces, however, introduced a polarization of $\sim 3\%$ into the unpolarized component of the light. Then, assuming the same field dependence of the intensity, the signal produced by the lock-in amplifier has the form

$$(1-C^2H^2) \left[-dI_o + \frac{P_o}{1+(2\mu H\tau)^2} \right]$$

so that the resultant signal has a fitted curve somewhat broader than the true Lorentzian. The effect is estimated

to produce changes in the apparent halfwidth not exceeding 1% for our curves.

b) Magnetic Field

The magnetic field calibration errors may be devided into non-linearities and miscalibration.

The magnetic field in the discharge region will in general not be quite proportional to the voltage across the coils. This is due partly to ohmic heating of the coils, and partly to hysteresis effects in nearby ferro-magnetic materials. Both of these effects should however be quite small in this experiment. In addition, the residual earth's field perpendicular to the applied field, causes a slight non-linearity. More serious are non-linearities in the x channel of the x-y recorder, i.e. pen displacements are not quite proportional to the field. The non-linearities introduce a maximum error of about 1% in $H_{1/2}$.

In addition to non-linearities the linear errors such as made in the reading of data from graphs represent another 1% random error. The gaussmeters available were only capable of measuring the magnetic field to an accuracy of .1 to .2 gauss. Thus a 2% systematic error - which does not effect the relative lifetimes of the states, but does affect the absolute lifetimes - arises.

Inhomogeneities of the magnetic field in the

discharge region were not measurable with our gausmeter and probably do not exceed .1 gauss leading to negligible broadening of the lineshapes.

The errors in the magnetic field will thus contribute about 3.5% error in the absolute lifetimes or 1.5% error in the relative lifetimes.

c) Pressure in the Discharge

It should be clear from FIG.10 that the pressure measured by the McLeod gauge will differ from the pressure in the discharge cell. We still expect the pressures to be proportional to those measured, so that we introduce no errors in the extrapolated lifetimes. For the cross-sections, however, the particle densities are needed. Pressure measurements inside the discharge cell would be difficult and accurate calculations equally difficult. Pressures in the discharge cell, should, judging from the proximity of the McLeod gauge, be no more than 20 or 30% less than those measured. The pressure difference is probably greatest for the liquid nitrogen cooled discharge.

d) Temperature in the Discharge

The temperature of the gas in the discharge again affects only the calculated cross-section. The mean free path of ground state H₂ at 50 μ pressure and 100°K temperature is of the order of the size of the discharge

cell, and the time between collisions is of order 10^{-5} seconds hence we expect translational equilibrium to be rapidly established with the walls of the discharge cell. Assuming a power input to the cell of 10W, and a thermal conductivity of pyrex of .01 Watts $\text{cm}^{-2}\text{cm}^{-1}/^\circ\text{K}$, the inside walls will be at a temperature about 2°K higher than the outside wall. Since the outside walls exhibit no great temperature rise when the pressure inside is less than 200 - 300 microns, it is inferred that the gas in the discharge will have a temperature not exceeding the ambient temperature by more than 10°K . As the computed cross-section varies as \sqrt{T} , a 10°K error in the assumed temperature will affect the results only slightly.

e) Cascading

Although there is no direct evidence that the $3d^1\Sigma$ levels are not populated by radiative transitions from higher energy states, no such transitions have ever been observed. It seems likely therefore that these transitions occur with very much lower probability than excitation from the ground state.

f) Coherence Narrowing

When light emitted by one molecule is absorbed by another before leaving the discharge, the Hanle effect signal will be "narrower" than the lifetime would indicate because the composit system has a longer lifetime than

the individual molecules. This phenomenon does not occur in these levels because there are no electric dipole transitions to the ground state, nor is there a metastable state to which it can decay.

g) R.F. Broadening

The presence of R.F. fields will in general broaden the polarization curves. In the presence of a weak magnetic field, it is possible to take account of the Stark term, providing the R.F. frequency $v >> \omega_\mu - \omega_{\mu'}$, the Larmor frequency. The polarization curve then obtained is of the form⁷:

$$P = \frac{P_0}{\Gamma^2 + C^2 E^4 + (\omega_\mu - \omega_{\mu'})^2}$$

(compare with eq.(9)) where C is a constant depending on the polarizability of the state, but independent of v , and $\Gamma = \frac{1}{T}$. The apparent lifetime yielded from these curves is $\tau_{app} = \frac{1}{\sqrt{\Gamma^2 + C^2 E^4}}$

In this experiment an E of approximately 100-150V/cm and 300-400V/cm were used. Thus the factor $C^2 E^4$ is changed by a factor of at least 80, i.e. the correction that should be applied to τ_{app} is changed by a factor of 9. Since τ_{app} does not appear to decrease at the larger field, we conclude that $C^2 E^4 \ll \Gamma$ and $\tau = \tau_{app}$ within the experimental accuracy.

§4.6 Helium 4^1D Lifetime Compared With That Obtained From Other Experiments

Perhaps the most convincing proof that the lifetimes measured are not seriously affected by magnetic field inhomogeneities, R.F. fields and other broadening mechanisms would be to remeasure the lifetime of a state whose lifetime has already been determined by other workers using various methods. In particular a state with a narrower Hanle effect curve than those measured in this thesis should be chosen.

A convenient example of such a state is offered by the atomic Helium 4^1D state whose transitions $4^1D \rightarrow 2^1P$ occurs at 4922\AA . This transition is very bright compared to those observed in molecular hydrogen and has a relatively high polarization. The He 4^1D state has a lifetime of approximately 4×10^{-8} sec. and a Landé g factor of 1 so that its Hanle effect curve should be some 30% narrower than the narrowest of these observed for H₂ in this thesis.

A typical zero field level crossing effect curve for this state is shown in FIG.25. The curve extrapolating the halfwidth to zero pressure is shown in FIG.26. The lifetime thus obtained is $(3.97 \pm .4) \times 10^{-8}$ sec. In Table VIII, lifetimes obtained by various other workers are listed for comparison.

The experimental work on this line was performed by R.E. Bardsley of this laboratory.

$\tau (\times 10^{-8} \text{ sec})$	Author	Technique	Date
$3.8 \pm .3$	I. Martison et al. ³⁴	Beam foil	1969
$3.91 \pm .2$	Descomps et al. ³⁵	Magnetic Resonance	1960
$4.1 \pm .5$	J.P. Descoubes ³⁶	Level Crossing	1967
$4.7 \pm .5$	Pendleton and Hughes ³⁷	Direct observation of decay	1965
$3.0 \pm .5$	Kindleman and Bennett ³⁸	Delayed coincidence	1963
$3.5 \pm .4$	Fowler et al. ³⁹	Direct observation of decay	1964
$3.9 \pm .5$	Bridgett and King ⁴⁰	Direct observation of decay	1967
$3.8 \pm .5$	Allen et al. ⁴¹	Direct observation of decay	1969
3.66	Wiese et al. ⁴²	Theoretical	1965
$3.97 \pm .4$	ours	Level Crossing	

Table VIII - Lifetime of the 4^1D State of Helium

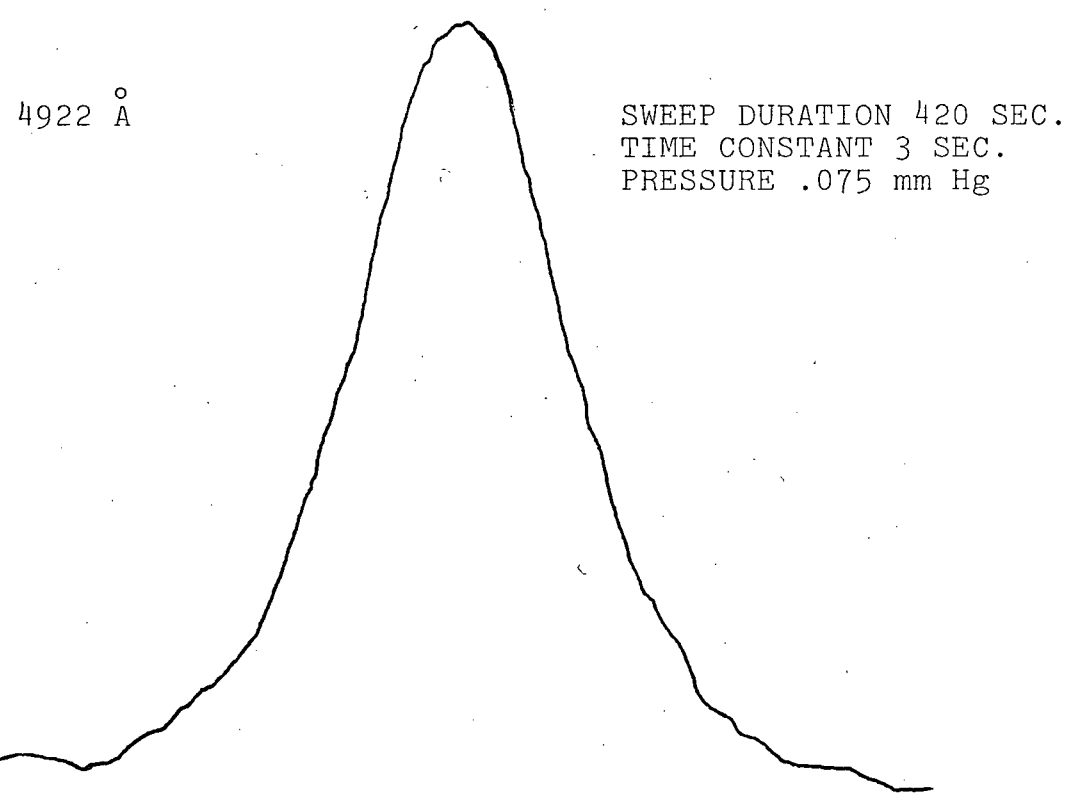


Figure 25 - Experimental Level-Crossing Curve for the Helium $4^1D \rightarrow 2^1P$ Transition

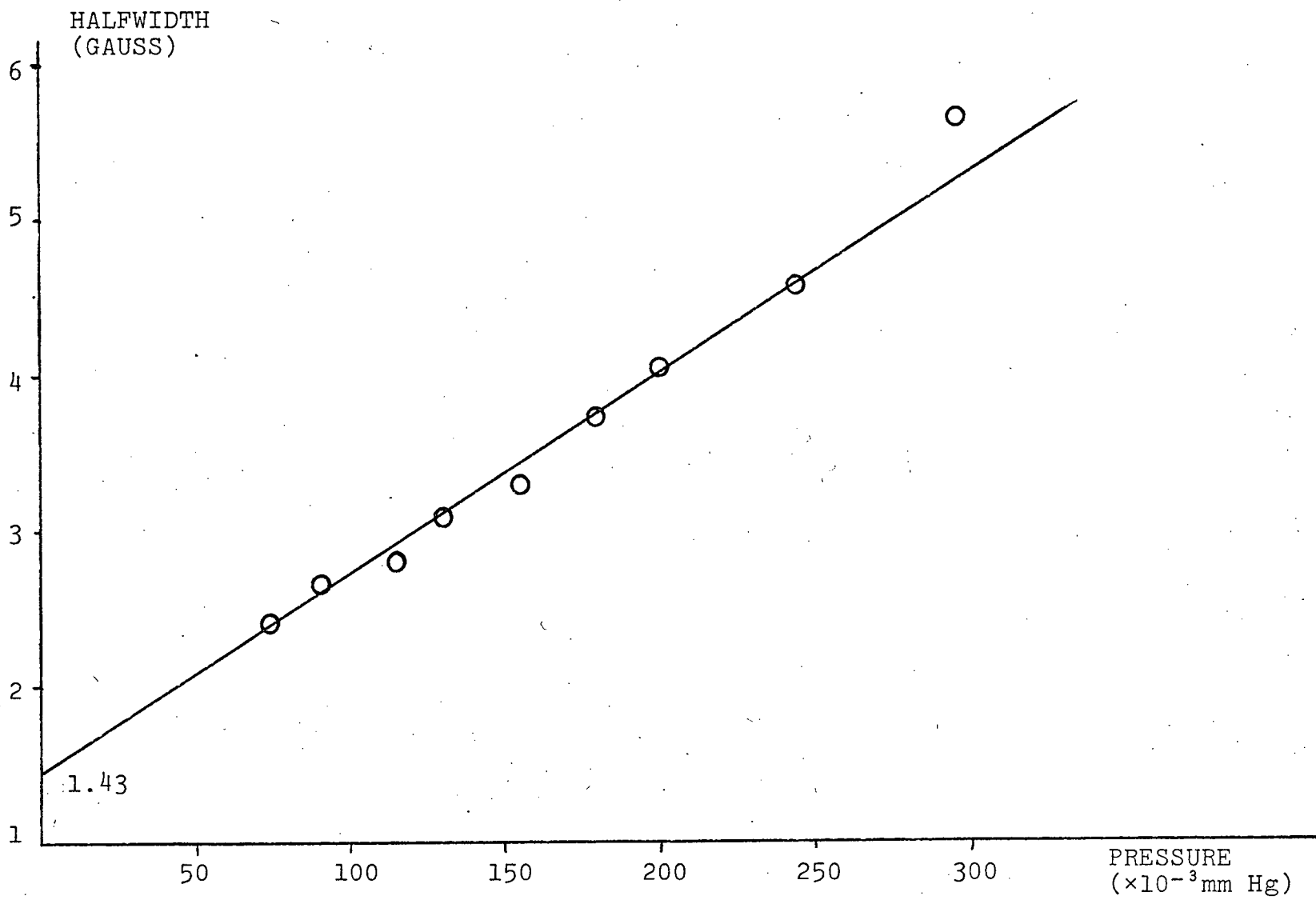


Figure 26 - ${}^4\text{D}$ Curve Halfwidth as a Function of Pressure

CHAPTER V

DISCUSSION OF RESULTS AND CONCLUSION

§5.1 Introduction

Under the Born-Oppenheimer approximation we expect the lifetime of a state to depend primarily on the electronic and vibrational parts of the wave function and only very weakly on the rotational part of the wave function. For the states measured, however, there appears to be a large discrepancy between the lifetimes of the $J=1$ state $[(2.66 \pm .1) \times 10^{-8} \text{ sec}]$ and the lifetimes of the $J=2$, and 3 states $[(3.85 \pm .15) \times 10^{-8} \text{ sec}]$. The question naturally arises, whether this discrepancy is real, and, if it is, how might we account for it.

§5.2 Hyperfine Effects

We will first consider whether this lifetime discrepancy could be real. It seems very unlikely that there are experimental errors large enough to account for the 50% discrepancy in lifetimes, we will therefore re-examine the theory. Primary requirements for the application of the theory to this experiment are that the Zeeman effect be linear and that the Landé g factor be known. Throughout this discussion we have ignored the effect of non-zero nuclear spin on the Zeeman effect. As is well known, in the absence of an external field, the nuclear spin I couples to J to form a total angular momentum $F=I+J$, $I+J-1, \dots, |I-J|$. When a large magnetic field is applied they become decoupled and precess

seperately about the field. The g factor, g_F , at very low fields is related to the high field g factor g_J by

$$g_F = \frac{F(F+1) + J(J+1) - I(I+1)}{2F(F+1)} g_J$$

For the $J=1$ state this yields

$$g_F = \frac{1}{2} g_J$$

and using g_F to compute the lifetime $\tau = (5.32 \pm .2) \times 10^{-8}$ sec. which is now much too large compared to the $J=2$ lifetime ($J=2$ has $I=0$ so that $g_F=g_J$).

Besides the two limiting cases of the magnetic field dependence of the energy levels we may consider the intermediate case where the Zeeman effect is non-linear. We consider the Hamiltonian \mathcal{H} of a system in a magnetic field H , with angular momenta I and J coupled with a coupling parameter α .

$$\mathcal{H} = \mu_0 \underline{J} \cdot \underline{H} + \mu_n \underline{I} \cdot \underline{H} + \alpha \underline{I} \cdot \underline{J}$$

where μ_n is the nuclear magneton and as zero order eigenfunctions we take those at high field i.e.

$$|J, I, m_J, m_I\rangle$$

The non-zero matrix elements of this Hamiltonian are

$$\langle J, I, m_J, m_I | \mathcal{H} | J, I, m_J, m_I \rangle = \mu_0 m_J H + \mu_n m_I H + \alpha m_I m_J$$

and

$$\langle J, I, m_J, m_I | \mathcal{H} | J, I, m_J^{\pm 1}, m_I^{\mp 1} \rangle = \sqrt{J(J+1)-m_J(m_J^{\pm 1})} \cdot$$

$$\cdot \sqrt{I(I+1)-m_I(m_I^{\mp 1})}$$

The secular equation may be resolved into separate systems of dimension $\leq 2I+1$, whose eigenvalues are the energies and whose eigenvectors are the states of the system.

Neglecting the small term $\mu_n m_I H$ the secular equations are:
for $J=1$

$$E \pm \mu_J H - \alpha = 0 \quad \text{for the states} \quad |J, I, \pm l, \pm l\rangle$$

(i.e. these are already eigenstates of the system)

$$\begin{array}{cc|ccc|c} m_J = \pm 1 & & m_J = 0 & & & \\ m_I = 0 & & m_I = \pm 1 & & & \\ \hline m_J = \pm 1 & \pm \mu_J H - E & \alpha & & & = 0 \\ m_I = 0 & & & & & \\ \hline m_J = 0 & \alpha & -E & & & \\ m_I = \pm 1 & & & & & \end{array}$$

and

$$\begin{array}{ccc|ccc|c} m_J = -1 & m_J = 0 & m_J = 1 & & & & \\ m_I = 1 & m_I = 0 & m_I = -1 & & & & \\ \hline m_J = -1 & -\mu_J J - \alpha - E & \alpha & 0 & & & = 0 \\ m_I = 1 & & & & & & \\ \hline m_J = 0 & \alpha & -E & \alpha & & & \\ m_I = 0 & & & & & & \\ \hline m_J = 1 & 0 & \alpha & \mu_J H - \alpha - E & & & \end{array}$$

The roots of these equations are shown as a function of magnetic field in FIG.27. States that can interfere to produce level crossing effects are connected by double ended arrows.

We substitute the field dependent wave functions and energies into the Breit formula, and use the selection rule $\Delta m_I = 0$ (this merely says that the $I \cdot J$ coupling is so weak that the time involved in changing $m_I \gg \tau$). If for the excitation we again use the electric quadrupole moment $Q_{xx}^{(2)}$ we find after some lengthy calculations that the Lorentzian can indeed be broadened by an α of .5 to 10 MHz without seriously distorting the lineshape. The dispersive shape, obtained when the angle ϕ (see (§2.5) is changed to 45° , shows major distortions near $H=0$ for such an α . No such distortions have been observed experimentally.

It should be emphasized that the magnitude of the distortion depends on the excitation matrix elements; since ours are only qualitative, we can not rule out entirely hyperfine splittings comparable with the natural linewidth.

For the $J=3$ state the g factors g_F for $F=2, 3$, and 4 are respectively $\frac{4}{3}g_J$, $\frac{11}{12}g_J$, and $\frac{3}{4}g_J$. If the 3 F states are well resolved, the average g factor of these states is .95 g_J , and assuming that each contributes to the signal equally the width observed would be expected to be much the same.

The intermediate coupling case requires the handling

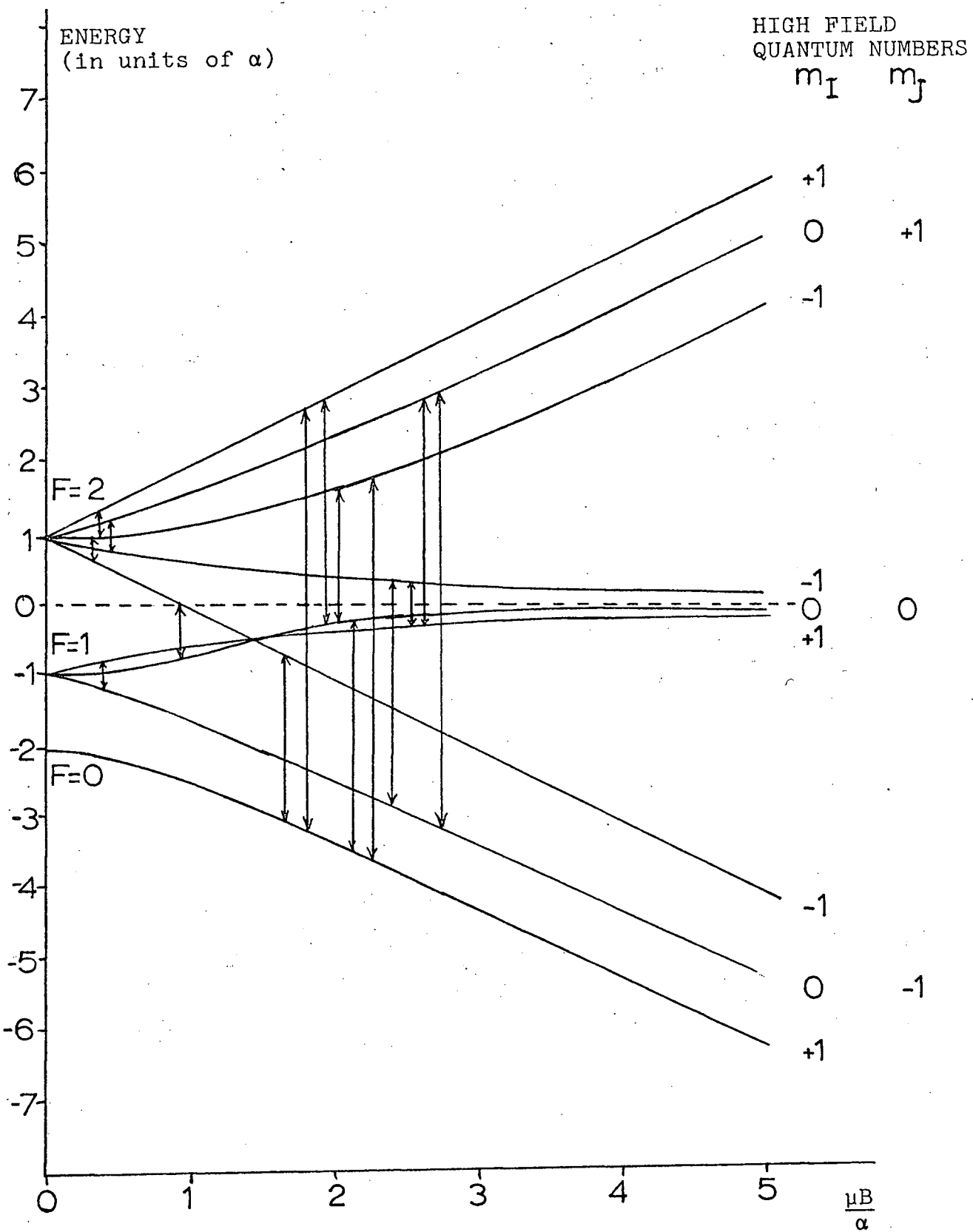


Figure 27 - Zeeman Effect in the Presence of Small Hyperfine Splitting

of 21 states and the labor involved is not warranted by the present data.

§5.3 Electronic Wave Function Variation with J

If we assume that the lifetime discrepancy is real, we must attribute it to the failure of the Born-Oppenheimer approximation. As mentioned in Chapter II, the $3d^1$ states of H_2 suffer from L-decoupling. The state vectors of the $3d^1\Sigma$ states are derived as linear combinations of the Hund's case b coupled Σ , Π and Δ states in Appendix II. i.e.

$$|\Sigma'(J)\rangle = A_\Sigma(J)|\Sigma\rangle + B_\Sigma(J)|\Pi\rangle + C_\Sigma(J)|\Delta\rangle$$

where the A_Ψ are the expansion coefficients and $|\Psi\rangle$ are the case b coupled states. Now using

$$\frac{1}{\tau_\Sigma(J)} = \frac{A_\Sigma(J)}{\tau_\Sigma} + \frac{B_\Sigma(J)}{\tau_\Pi} + \frac{C_\Sigma(J)}{\tau_\Delta}$$

we attempt to solve for τ_Σ , τ_Π , and τ_Δ . Using the τ obtained assuming zero hyperfine splitting, solutions to any pair of these equations exist only if at least one of the τ 's is negative. Hence it is clear that under the simple coupling scheme considered we cannot explain the lifetime discrepancy.

If for the lifetimes we use those obtained assuming a large hyperfine splitting compared to the natural width, the equations are soluble and yield $\tau_\Sigma \sim 8 \times 10^{-8}$ sec. and $\tau_\Pi \sim 4.5 \times 10^{-8}$ sec. But now, using $g_F = .450$ for the $J=1$ state, the collision crosssection of the $J=1$ state becomes only half of that of the $J=2$ and $J=3$ states which seems rather unlikely.

In addition to the simple coupling scheme considered in Appendix II, there may be "mixed" into the states a very small fraction of a state with a very short lifetime. The mixing would have to be greater for $J=1$ than for $J=2$ and $J=3$ which is rare but not impossible.

§5.4 Conclusion and Suggestions for Further Work

This thesis has reported the first measurement of the molecular hydrogen $3d^1\Sigma$ state lifetimes and their collision cross-sections. The lifetimes are similar to that of the 3^1D state of Helium as expected. An apparent discrepancy between the lifetime of the $J=1$ state and those of the $J=2$ and $J=3$ states may possibly be accounted for if one assumes a hyperfine splitting of a few MHz in the excited states $J=1$ and $J=3$; no evidence of this was obtained in this thesis. Because the $J=2$ state lacks any hyperfine structure, its lifetime is the only one that can be accepted with certainty. It is suggested that some of the ambiguity in the interpretation of the results for the $J=1$ and $J=3$ states may be removed by searching for a non-zero field level crossing, preferably with the hyperfine levels of the $J=1$ state. This level crossing would be observable only if the hyperfine splitting exceeds 20 MHz or so.

This method of measuring lifetimes should be applicable to almost any molecular or atomic lifetime providing the state involved has a $g\tau$ product in the range 10^{-7} sec to 10^{-10} sec. Refinements to the equipment could probably extend this range considerably.

APPENDIX I
THE TRANSITION MATRIX ELEMENTS

To compute the factors A and R_0 in the Breit formula, we shall need for the excitation the matrix elements of the quadrupole moment, $Q_{xx}^{(2)}$, and for the decay those of the dipole moment, $\underline{g} \cdot \underline{r}$.

The element $Q_{xx}^{(2)}$ of the quadrupole moment tensor may be rewritten in terms of spherical harmonics, $Y_{\ell m}$, whose matrix elements are well known³¹. In particular

$$Q_{xx}^{(2)} \propto -Y_{2,2} - Y_{2,-2} + \sqrt{\frac{2}{3}} \cdot Y_{2,0}$$

abbreviating

$$\langle J, m | Y_{\ell m} | J', m' \rangle = \left[Y_{\ell m} \right]_{J', m'}^{J, m}$$

$$\left[Y_{2,0} \right]_{J, m}^{J, m} = 2[3m^2 - J(J+1)] \left[Y_2 \right]_J^J$$

$$\left[Y_{2,0} \right]_{J+2, m}^{J, m} = [6(J+m+2)(J+m+1)(J-m+2)(J-m+1)]^{1/2} \left[Y_2 \right]_{J+2}^J$$

$$\left[Y_{2, \pm 2} \right]_{J, m \mp 2}^{J, m} = [6(J \pm m - 1)(J \pm m)(J \mp m + 1)(J \mp m + 2)]^{1/2} \left[Y_2 \right]_J^J$$

$$\left[Y_{2, \pm 2} \right]_{J+2, m \mp 2}^{J, m} = [(J \pm m + 1)(J \pm m + 2)(J \pm m + 3)(J \pm m + 4)]^{1/2} \left[Y_2 \right]_{J+2}^J$$

where the factors $\left[Y_2 \right]_J^J$ are reduced matrix elements independent of the magnetic quantum numbers. Because they enter into

A and R_0 only as common factors they will be ignored henceforth and set equal to unity.

The dipole moment operator is similarly expanded into the familiar raising and lowering operator. Letting ϕ be the angle \underline{g} makes with the x -axis:

$$\underline{g} = \hat{g}_i \cdot \cos\phi + \hat{g}_j \cdot \sin\phi$$

then $\underline{g} \cdot \underline{r} \propto r_x \cos\phi + r_y \sin\phi$

and setting $R_{\pm} = r_x \pm i r_y$

or $r_x = \frac{R_+ + R_-}{2}$ and $r_y = \frac{R_+ - R_-}{2i}$

The matrix elements of R_{\pm} are:

$$(R_{\pm})_{J-1, m \pm 1}^{J, m} = [(J \pm m)(J \pm m - 1)]^{1/2} R_{J-1}^J = (R_{\mp})_{J, m}^{J-1, m \mp 1}$$

Again we will neglect the common factor R_{J-1}^J in all subsequent calculations. Referring to eq.(7) (§2.3) we see that in the terms A , $\mu > \mu'$; since both states decay to a state v with $v = \mu \pm l = \mu' \pm l$ we find that $v = \mu' + l$ and $\mu = \mu' + 2$

so that $(r_x)_v^{\mu'} = (R_-)_{\mu'+1}^{\mu'} \quad (r_y)_v^{\mu'} = (iR_-)_{\mu'+1}^{\mu'}$

$$(r_x)_\mu^v = (R_-)_{\mu'+2}^{\mu'+1} \quad (r_y)_\mu^v = (iR_-)_{\mu'+2}^{\mu'+1}$$

Thus

$$g_{\mu, v} = (A_-)_v^{\mu'} e^{i\phi}$$

$$g_{v\mu} = (A_-)_\mu^v e^{i\phi}$$

Specific Applications

The line $R(0)$ arises from the transition sequence

$$J_1 \rightarrow J'_1 \rightarrow J''_0 \quad \text{i.e. } v=0, \mu=1, \mu'=-1, \text{ and } m=\pm 1$$

For $m=-1$

$$Q_{\mu m} Q_{m\mu'} = -(Y_{2,2})_{1,-1}^{1,1} \sqrt{\frac{2}{3}} (Y_{2,0})_{0,-1}^{1,-1} = -8$$

$$g_{\mu',v} g_{v\mu} = (R_-)_{0,0}^{1,-1} (R_-)_{1,1}^{0,0} e^{2i\phi} = -2e^{2i\phi}$$

$$\text{thus } A(1,\mu,\mu',v) = 16e^{2i\phi}$$

For $m=+1$

$$Q_{\mu m} Q_{m\mu'} = - \sqrt{\frac{2}{3}} (Y_{2,0})_{1,1}^{1,1} (Y_{2,2})_{1,-1}^{1,1} = -8$$

$$g_{\mu',v} g_{v\mu} = 2e^{2i\phi}$$

$$\text{and } A(+1,\mu,\mu',v) = 16e^{2i\phi}$$

$$\text{thus } \sum_{m>\mu'} \sum_{m>\mu} A(m,\mu,\mu',v) = 32e^{2i\phi}$$

$$\begin{aligned} R_0 &= |Q_{-1,-1}|^2 |g_{-1,0}|^2 + |Q_{-1,1}|^2 |g_{1,0}|^2 + |Q_{1,-1}|^2 |g_{-1,0}|^2 + \\ &\quad + |Q_{1,1}|^2 |g_{1,0}|^2 \\ &= 101.3 \end{aligned}$$

$$\text{Hence } P_0 = .632$$

The line $R(2)$ arises from the sequence $J_0 \rightarrow J'_2 \rightarrow J''_1$

$$\text{i.e. } \begin{cases} \mu' = -2 \\ \mu = 0 \end{cases} \Rightarrow v = -1$$

$$m=0,$$

$$\begin{cases} \mu' = 0 \\ \mu = 2 \end{cases} \Rightarrow v = 1$$

$$\sum_{m\mu > \mu'} \sum A(m, \mu, \mu', -1) = 96 e^{2i\phi}$$

similarly

$$\sum_{m\mu > \mu'} \sum A(m, \mu, \mu', +1) = 96 e^{2i\phi}$$

$$\sum_{m\nu\mu > \mu'} \sum A(m, \mu, \mu', \nu) = 192 e^{2i\phi}$$

and $R_o = 640$

$$\text{hence } P_o = \frac{192}{320} = .6$$

The transition $R(2)$ arises from the sequence $\begin{matrix} J \\ 1 \end{matrix} \rightarrow \begin{matrix} J' \\ 3 \end{matrix} \rightarrow \begin{matrix} J'' \\ 2 \end{matrix}$

The non-zero combinations of matrix elements here are:

$$\begin{array}{ccccc} m & \rightarrow & \begin{matrix} \mu \\ \mu' \end{matrix} & \rightarrow & \nu \\ -1 & \rightarrow & \begin{matrix} -1 \\ -3 \end{matrix} & \rightarrow & -2 \\ -1 & \rightarrow & \begin{matrix} 1 \\ -1 \end{matrix} & \rightarrow & 0 \\ 1 & \rightarrow & \begin{matrix} 3 \\ 1 \end{matrix} & \rightarrow & 2 \\ 1 & \rightarrow & \begin{matrix} 1 \\ -1 \end{matrix} & \rightarrow & 0 \\ 0 & \rightarrow & \begin{matrix} 2 \\ 0 \end{matrix} & \rightarrow & 1 \\ 0 & \rightarrow & \begin{matrix} 0 \\ -2 \end{matrix} & \rightarrow & -1 \end{array}$$

and making the usual substitutions,

$$\sum_{\mu > \mu'} A(\pm 1, \mu, \mu', \pm 2) = 1540\sqrt{14} e^{2i\phi}$$

$$\sum_{\mu > \mu'} A(\pm 1, \mu, \mu', 0) = 576 e^{2i\phi}$$

$$\sum_{\mu > \mu'} A(0, \mu, \mu', \pm 1) = 1440 e^{2i\phi}$$

or $\sum_{m\nu\mu > \mu'} \sum A(m, \mu, \mu', \nu) = 15,556 e^{2i\phi} \quad R_o = 112,992$

and $P_o = .275$

APPENDIX II

THE 3d¹ STATES OF H₂

§A2.1 Energy Levels and Eigenstates

The Hamiltonian for the rotating molecule may be written in the molecule fixed frame

$$\begin{aligned}\mathcal{H} &= E_{n,L,|\Lambda|,v} + B(J_x^2 - L_x^2)^2 + B(J_y^2 - L_y^2)^2 \\ &= E_{n,L,|\Lambda|,v} + B[J_x^2 + J_x^2 + L_x^2 + L_y^2 + 2J_x L_x + 2J_y L_y] \\ &= E_{n,L,|\Lambda|,v} + B[J^2 - J_z^2 + L^2 - L_z^2 + J^+ L^- + J^- L^+]\end{aligned}$$

where $B = \frac{\hbar^2}{2\mu r^2}$, r is the internuclear distance
 μ is the reduced mass

L is the electronic angular momentum

J is the total angular momentum in the molecule fixed frame

z is the internuclear axis

$$J^\pm = J_x \pm i J_y$$

$$L^\pm = L_x \pm i L_y$$

Using Hund's case b basis functions and assuming "pure precession", the non-zero matrix elements of \mathcal{H} are³²:

$$\langle L, \Lambda, J | \mathcal{H} | L, \Lambda \pm 1, J \rangle = B[L(L+1) - \Lambda(\Lambda \pm 1)]^{1/2} \cdot [(J \mp \Lambda)(J \pm \Lambda + 1)]^{1/2}$$

$$\langle L, \Lambda, J | \mathcal{H} | L, \Lambda, J \rangle = B[J(J+1) - \Lambda^2 + L(L+1) - \Lambda^2]$$

Hence for the 3d¹ system the states $|J, \Lambda\rangle$ of interest are

$$|J, \pm 2\rangle = |\Delta_\pm\rangle$$

$$|J, \pm 1\rangle = |\Pi_\pm\rangle$$

$$|J, 0\rangle = |\Sigma\rangle$$

For these states the matrix elements are:

$$\alpha = \langle \Sigma | \mathcal{H} | \Sigma \rangle = B_{\Sigma} [J(J+1)] + E_{\Sigma}$$

$$\beta = \langle \Pi_{\pm} | \mathcal{H} | \Pi_{\pm} \rangle = B_{\Pi} [J(J+1)-2] + E_{\Pi}$$

$$\delta = \langle \Delta_{\pm} | \mathcal{H} | \Delta_{\pm} \rangle = B_{\Delta} [J(J+1)-6] + E_{\Delta}$$

$$\epsilon = \langle \Sigma | \mathcal{H} | \Pi_{\pm} \rangle = B_{\Sigma\Pi} [J(J+1)L(L+1)]^{1/2}$$

$$\eta = \langle \Pi_{\pm} | \mathcal{H} | \Delta_{\pm} \rangle = B_{\Pi\Delta} [(J+2)(J-1)(L+2)(L-1)]^{1/2}$$

We then obtain the eigenvalue equation:

$$\begin{pmatrix} \alpha & \epsilon & \epsilon & 0 & 0 \\ \epsilon & \beta & 0 & \eta & 0 \\ \epsilon & 0 & \beta & 0 & \eta \\ 0 & \eta & 0 & \delta & 0 \\ 0 & 0 & \eta & 0 & \delta \end{pmatrix} \begin{pmatrix} A_{\lambda} \Sigma \\ B_{\lambda} \Pi_+ \\ C_{\lambda} \Pi_- \\ D_{\lambda} \Delta_+ \\ F_{\lambda} \Delta_- \end{pmatrix} = \lambda \cdot \begin{pmatrix} A_{\lambda} \Sigma \\ B_{\lambda} \Pi_+ \\ C_{\lambda} \Pi_- \\ D_{\lambda} \Delta_+ \\ F_{\lambda} \Delta_- \end{pmatrix}$$

Transforming to a system of symmetric and anti-symmetric wave functions:

$$\Pi^{\pm} = \frac{1}{\sqrt{2}}(\Pi_+ \pm \Pi_-)$$

$$\Delta^{\pm} = \frac{1}{\sqrt{2}}(\Delta_+ \pm \Delta_-)$$

The above equation becomes, after some rearrangement of the terms:

$$\begin{pmatrix} \alpha & \sqrt{2}\epsilon & 0 & 0 & 0 \\ \sqrt{2}\epsilon & \beta & \eta & 0 & 0 \\ 0 & \eta & \delta & 0 & 0 \\ 0 & 0 & 0 & \beta & \eta \\ 0 & 0 & 0 & \eta & \delta \end{pmatrix} \begin{pmatrix} A_{\lambda}^+ \Sigma \\ B_{\lambda}^+ \Pi^+ \\ C_{\lambda}^+ \Delta^+ \\ B_{\lambda}^- \Pi^- \\ C_{\lambda}^- \Delta^- \end{pmatrix} = \lambda \cdot \begin{pmatrix} A_{\lambda}^+ \Sigma \\ B_{\lambda}^+ \Pi^+ \\ C_{\lambda}^+ \Delta^+ \\ B_{\lambda}^- \Pi^- \\ C_{\lambda}^- \Delta^- \end{pmatrix}$$

whose solutions yield the energies and state vectors of the system.

The energies of the Σ and Π state in the absence

of any $J \cdot L$ coupling are unambiguously known since $\Sigma(J=0)$ and $\Pi^-(J=1)$ are unperturbed.

Thus $E_{\Sigma} = 111,804.63 \text{ cm}^{-1}$
and $E_{\Pi} = 112,064.91 \text{ cm}^{-1}$

The observed spectrum can then be used to find B_{Σ} , B_{Π} , B_{Δ} , $B_{\Sigma\Pi}$, $B_{\Pi\Delta}$, and E_{Δ} .

The best values obtained by trial-and-error were:

$$\begin{aligned} E_{\Delta} &= 112,488 \text{ cm}^{-1} \\ B_{\Sigma} &= 27.2 \text{ cm}^{-1} \\ B_{\Pi} &= 27.76 \text{ cm}^{-1} \\ B_{\Delta} &= 28.11 \text{ cm}^{-1} \\ B_{\Sigma\Pi} &= 26.39 \text{ cm}^{-1} \\ B_{\Pi\Delta} &= 27.54 \text{ cm}^{-1} \end{aligned}$$

The energies thus found for the states are listed in Table IX. The energies given by Dieke¹⁸ are also listed for comparison. The fit of these energies can probably be somewhat improved, particularly at high J , by inclusion of the centrifugal distortion term $-D_v J^2 (J+1)^2$. A value of .02 for D_o fits the Σ state data well.

Corresponding to the energy eigenvalues found above, the eigenstates of the system may now be found in terms of the "pure" states Σ, Π^\pm , and Δ^\pm . Denoting the eigenstates Σ' , $(\Pi^\pm)'$, $(\Delta^\pm)'$ according to which state they tend as $B_{\Pi\Delta} \rightarrow 0$ and $B_{\Sigma\Pi} \rightarrow 0$:

$$\begin{aligned} \Sigma' &= A_{\Sigma} |\Sigma\rangle + B_{\Sigma} |\Pi^+\rangle + C_{\Sigma} |\Delta^+\rangle \\ (\Pi^+)' &= A_{\Pi} |\Sigma\rangle + B_{\Pi} |\Pi^+\rangle + C_{\Pi} |\Delta^+\rangle \\ (\Delta^+)' &= A_{\Delta} |\Sigma\rangle + B_{\Delta} |\Pi^+\rangle + C_{\Delta} |\Delta^+\rangle \end{aligned}$$

J	Energy from above theory (cm ⁻¹)	Observed energy (cm ⁻¹)	Energy from above theory (cm ⁻¹)	Observed energy (cm ⁻¹)
Σ				
0	111804.63	111804.63		
1	1796.64	1797.11		
2	1819.54	1819.78		
3	1888.90	1885.07		
4	2009.38	1997.49		
Π^+				
1	112127.50	112127.23	112064.91	112064.91
2	2279.27	2274.24	2140.99	2139.61
3	2472.01	2463.04	2265.06	2264.09
4	2709.58	2695.70	2440.74	2441.12
5			2669.87	2671.10
6			2953.38	2953.21
Δ^+				
2	112533	112528.75	112522.96	112517.95
3	2769	2766.60	2734.12	2735.56
4	3075	3070.18	3005.42	3010.39
5			3335.01	3338.57
6			3721.97	3716.85

Table IX - Energies of the 3d¹ Complex of H₂

The coefficients A_ψ, B_ψ, C_ψ, for the first six rotational levels of the symmetrized states Σ' , $(\Pi^+)'$, and $(\Delta^+)'$ are listed in Table X.

Using these expansions, another check on these wave functions is provided by the ratios of the intensities of the

J	A_{Σ}	B_{Σ}	C_{Σ}	A_{Π}	B_{Π}	C_{Π}	A_{Δ}	B_{Δ}	C_{Δ}
1	.901	-.434	0	.434	.901	0	0	0	0
2	.830	-.550	.090	.537	.746	-.394	.148	.375	.915
3	.787	-.602	.137	.560	.603	-.569	.260	.524	.811
4	.759	-.629	.169	.557	.492	-.669	.338	.602	.724
5	.739	-.646	.192	.550	.413	-.726	.389	.642	.660
6	.725	-.657	.210	.543	.357	-.760	.424	.664	.616

Table X - Expansion Coefficients for the $3d^{1+}$ States

R and P lines arising from the same upper state. Because the B values of the states are almost identical the Franck-Condon factors will be almost identical and will be set to unity. The transition matrix elements, $A_{J' \rightarrow J''}$ for the $3d^1(\Sigma) \rightarrow 2p^1\Sigma$ will then be given by

$$A_{J' \rightarrow J''} = A_{\Sigma}(J) \langle \Sigma, J'' | P | \Sigma, J' \rangle + B_{\Sigma}(J) \langle \Sigma, J'' | P | \Pi, J' \rangle$$

where P is the dipole moment operator summed over all directions.

The individual matrix elements are given by J.K.L. MacDonald³³ as:

$$\langle \Sigma, J | P | \Sigma, J+1 \rangle = [4(J+1)/(2J+1)]^{1/2} \quad P(J+1)$$

$$\langle \Sigma, J | P | \Sigma, J \rangle = 0 \quad Q(J)$$

$$\langle \Sigma, J | P | \Sigma, J-1 \rangle = [4J/(2J+1)]^{1/2} \quad R(J-1)$$

$$\langle \Pi, J | P | \Sigma, J+1 \rangle = [3J/(2J+1)]^{1/2} \quad P(J+1)$$

$$\langle \Pi, J | P | \Sigma, J \rangle = \sqrt{3} \quad Q(J)$$

$$\langle \Pi, J | P | \Sigma, J-1 \rangle = -[3(J+1)/(2J+1)]^{1/2} \quad R(J-1)$$

The theoretical relative intensities thus found are listed in Table XI for the first six rotational states' transitions to the $2p^1\Sigma$ states. Those measured experimentally are also listed in Table XI for comparison.

The energy levels and relative intensities of lines are not stringent tests of the foregoing theory; the former because of the large number of parameters used to fit the data, the latter because of the experimental inaccuracy. A more sensitive test is offered by the Zeeman effect of these levels.

Transitions	I(Theor.)	I(Exptl.)		Theor.	Exptl.	
		80°K	300°K	$\frac{I_{R(J'-1)}}{I_{P(J'+1)}}$	$\frac{I_{R(J'-1)}}{I_{P(J'+1)}}$	80°K
R(0)	2.74	42	46	2.5	3.2	2.7
P(2)	1.07	13	17			
R(1)	3.20	40	33	6.8	8	6.6
P(3)	0.47	5	5			
R(2)	3.31	80	93	13	26	18.6
P(4)	.26	3	5			
R(3)	3.33			20		
P(5)	.16					
R(4)	3.32			26		
P(6)	.11					
R(5)	3.31			39		
P(7)	.09					

Table XI - Relative Intensities of P and R Transitions
in the $3d^1\Sigma \rightarrow 2p^1\Sigma (0,0)$ Band

§A2.2 The Zeeman Effect

The Zeeman effect Hamiltonian, \mathcal{H}_m , may be written

$$\mathcal{H}_m = \mu_0 \underline{\mathbf{L}} \cdot \underline{\mathbf{H}}$$

under Hund's case b coupling, the term $\underline{\mathbf{L}} \cdot \underline{\mathbf{H}}$ may be rewritten as

$$\underline{\mathbf{L}} \cdot \underline{\mathbf{H}} = \frac{(\underline{\mathbf{L}} \cdot \underline{\mathbf{J}})(\underline{\mathbf{J}} \cdot \underline{\mathbf{H}})}{J^2} = \frac{2L_Z J_Z + L^+ J^- + L^- J^+}{2J^2} \cdot \underline{\mathbf{J}} \cdot \underline{\mathbf{H}}$$

where L_z , J_z , L^\pm , and J^\pm are all referred to the molecule fixed frame. The non-zero matrix elements of \mathcal{H}_m are then (again assuming pure precession):

$$\langle \Lambda, J, m_J | \mathcal{H}_m | \Lambda, J, m_J \rangle = \frac{\mu_0 H \Lambda^2}{J(J+1)} m_J \equiv g_J(\Lambda, \Lambda) \mu_0 H m_J$$

$$\langle \Lambda, J, m_J | \mathcal{H}_m | \Lambda \pm 1, J, m_J \rangle = -\frac{\mu_0 H m_J}{2J(J+1)} \sqrt{L(L+1)-\Lambda(\Lambda \pm 1)} \sqrt{(J \mp \Lambda)(J \pm \Lambda + 1)}$$
$$\equiv g_J(\Lambda, \Lambda \pm 1) \mu_0 H m_J$$

To solve now for the energies of the states in a magnetic field, we can follow either of two courses. \mathcal{H}_m may be added to \mathcal{H} (§A2.1) and the perturbation matrix diagonalized again. This procedure would be necessary if the energy splittings due to the magnetic field were comparable to the zero-field splittings. Although this is not the case for our states, there is an interesting conclusion that can be drawn from this procedure. Let us in particular look at a complete set of states with common J and $m_J = 1$. The trace (sum of the diagonal elements) of the non-diagonalized matrix is then just the sum of the zero-field energies and the $g_J(\Lambda, \Lambda) \mu_0 H$ products. Diagonalization of the matrix leaves the trace invariant, hence under any coupling scheme, the sum $\sum g_J = \sum g_J(\Lambda, \Lambda)$ where the summation takes place over all coupled states. This conclusion is independent of any coupling parameters and serves as a test to determine whether the set of states considered is a complete set.

The argument above does not yield information on the individual g -factors unless the complete diagonalization is carried out. A simpler procedure for finding g_J under the coupling scheme considered in §A2.1 is to use non-degenerate first order perturbation theory with the perturbation Hamiltonian \mathcal{H}_m .

Thus; for the Σ' state

$$\begin{aligned}
 g_J &= \frac{1}{Hm_J \mu_0} \langle \Sigma', J, m_J | \mathcal{H}_m | \Sigma', J, m_J \rangle \\
 &= A_{\Sigma}^2(J)g_J(\Sigma, \Sigma) + B_{\Sigma}^2(J)g_J(\Pi^+, \Pi^+) + C_{\Sigma}^2(J)g_J(\Delta^+, \Delta^+) \\
 &\quad + A_{\Sigma}(J)B_{\Sigma}(J)[g_J(\Sigma, \Pi^+) + g_J(\Pi^+, \Sigma)] \\
 &\quad + B_{\Sigma}(J)C_{\Sigma}(J)[g_J(\Pi^+, \Delta^+) + g_J(\Delta^+, \Pi^+)]
 \end{aligned}$$

The g factors thus found for the first six rotational levels of the Σ' state using the coefficients from Table X are listed in Table XII.

J	g-theory	g-experimental
1	.771	.901
2	.541	.571
3	.409	.455
4	.320	.387
5	.245	.331
6	.233	.287

Table XII - g -values of the $3d^1\Sigma$ State

The g factors derived above, although showing a qualitative agreement with those experimentally obtained³⁰, do not fit the data nearly as well as might be expected. It is worthwhile to examine whether the Σ , Π , and Δ states considered do form a complete basis. The pure case b coupled states have g -factors $\frac{\Lambda^2}{J(J+1)}$. Hence for the $J=1$ states, the sum of the g -factors is 0.5. Looking at Dieke's experimental data,

$g_1(\Sigma) = \pm .901$ and $g_1(\Pi^+) = \pm .500$. There appears to be no way that these g-factors can be added to give a 0.5 sum; we can therefore conclude that our set of basis functions is not complete. The addition of other vibrational levels to the set will not help as the overlap integral of the vibrational wavefunctions $B_{\Lambda,v;\Lambda',v'}$ for $v=v' \pm 1$ should be quite small. Other candidates for inclusion in the perturbation treatment include the 3^1K level, a ${}^1\Sigma$ state with both electrons excited, which shows a small Zeeman splitting.

In order to ensure that the g-factors reported by Dieke³⁰ were not the result of arithmetic or measuring errors, the spectrum of H₂ in a 24,500 gauss field was photographed on a Jarrel-Ash 3m grating spectrograph. A reproduction of a portion of the plate showing the R(0), R(1) and R(2) lines with polaroid perpendicular (a), and parallel (b) to the field is shown in FIG. 28.

The g-factors, g_J obtained from the R(0), R(1), and R(2) lines are:

$$g_1 = .900$$

$$g_2 = .597$$

$$g_3 = .452$$

It should be mentioned that as R(4) overlaps R(1), the splitting measured is open to question. These values are in good agreement with those of Dieke.

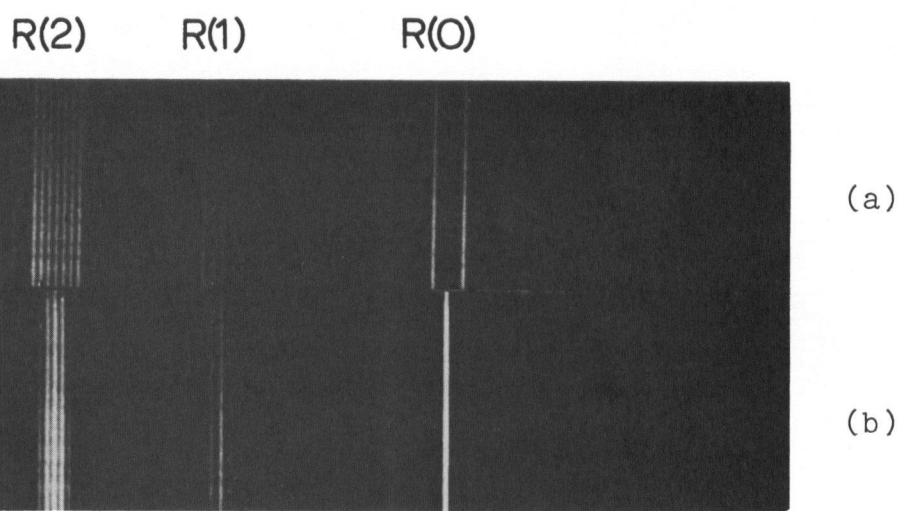


Figure 28 - The First Few Lines of the R Branch of
the $3d^1\Sigma \rightarrow 2p^1\Sigma(0,0)$ band of H_2

APPENDIX III

OTHER STATES

In addition to the work done on the $3d^1\Sigma$ states discussed before, some preliminary work was also done on the $3^1K(v=2)$ $J=1$, 2, and 3 levels and on the $3d^1\Pi^-(v=0)$ $J=2$ level.

§A3.1 The $3d^1\Pi^-(v=0)$ $J=2$ State

It was felt that a rough knowledge of the lifetime of the $3d^1\Pi$ and $3d^1\Delta$ would be useful in determining the reason for the discrepancy in the $3d^1\Sigma$ $J=1$, and the $J=2$ and 3, lifetimes. The brightest, most easily resolved line is the Q(2) $3d^1\Pi \rightarrow 2p^1\Sigma(0 \rightarrow 0)$. The polarization of this line is negative. Data was obtained for this line at pressures of 30μ and 20μ . The extrapolation of the halfwidth is subject to rather large errors, but as only a rough estimate ($\pm 20\%$) is required they should suffice. The halfwidths obtained are $4.805 \pm .045$ gauss at 30μ pressure, and $4.385 \pm .026$ gauss at 20μ pressure. These halfwidths are the average of 5 runs each and the errors quoted are statistical only. The extrapolation yields a zero-pressure halfwidth of $36 \pm .3$ gauss. The slope, $\frac{dH_{1/2}}{dp}$, suggests a cross-section of $\sim 170\text{\AA}^2$. The lifetime using Dieke's g-value of .412 is then 3.84×10^{-8} sec. The individual halfwidths of the line obtained on each run are listed in Table III.

Q(2) of $3d^1\Pi \rightarrow 2p^1\Sigma$

Pressure	30μ	20μ
	4.75458	4.37138
	4.81734	4.37775
	4.68231	4.40187
	4.90070	4.30700
	4.87179	4.52766
Average	$4.805 \pm .045$	$4.385 \pm .026$

Pressure	30μ	$3^1K \rightarrow 2p^1\Sigma$	
Transition	R(0)	R(1)	R(2)
	3.01	4.23	5.88
	3.51	4.25	6.29
	3.22	4.13	5.97
	3.26	3.97	5.61
	3.14	4.54	5.31
	3.14	4.13	5.59
Average	$3.21 \pm .08$	$4.21 \pm .08$	$5.77 \pm .15$

R(2) at 20μ has $H_{12} = 5.36$

30μ $H_{12} = 7.66$

Table III - Level Crossing Curve Halfwidths
($3d^1\Pi$ and 3^1K)

§A3.2 The 3^1K State

Although the information available on the 3^1K state has already been published^{4,3}, the data are listed in Table III. We attempted to measure the g-factor for these states with little success. The g-factor for the state $v=2$, $J=1$ is $.28 \pm .05$; the large error arises because the Zeeman pattern observed is only barely resolved and because long exposures were required which gave rise to somewhat distorted lineshapes. The splitting on the higher rotational lines could not be measured.

The lines observed are the R(0), R(1) and R(2) $3^1K(v=2) \rightarrow 2p^1\Sigma(v=5)$.

Only the R(2) line has had its halfwidth extrapolated to zero pressure; its $g\tau$ product is $(1.6 \pm .15) 10^{-8}$ sec. at zero pressure. Assuming a cross-section of 100\AA^2 , its g-factor is approximately .17 from which we would compute a lifetime of approximately 8×10^{-8} sec. Assuming the same lifetime and $g_1 = .28$, we obtain for the $J=1$ state a halfwidth at zero pressure of 2.46 gauss. Assuming the same cross-section for the $J=1$ state, the halfwidth extrapolated from 30μ to zero pressure, is 2.7 gauss. On the basis of our somewhat unwarrented assumptions this is in surprisingly good agreement.

REFERENCES AND FOOTNOTES

- 1 A.C.G. Mitchell and M.W. Zemansky; Resonance Radiation and Excited Atoms (Cambridge University Press, London, 1961) pp. 93-153.
- 2 G.M. Lawrence and D.B. Savage; Phys. Rev. 141, 67 (1966)
I. Brewer, C.G. James, R.G. Brewer, F.E. Stafford, R.M. Berg and G.M. Rosenblath; Rev. Sci. Instr. 23, 1450 (1962)
R.G. Bennett and F.W. Dalby; J. Chem. Phys. 40, 1414 (1964).
- 3 Only a few of the numerous papers are cited below:
P. Thaddeus and R. Novick; Phys. Rev. 136 A, 87 (1964)
J.P. Barratt; le Journal de Physique et la Radium 20, 633 (1959).
W. Demtröder; Zeits. f. Physik 166, 42 (1962).
- 4 D.R. Crossley and R.N. Zare; Phys. Rev. Letters 18, 942 (1967).
- 5 A. Marshall, R.L. de Zafra, H. Metcalf; Phys. Rev. Letters 22, 445 (1969)
K.R. German and R.N. Zare; Phys. Rev. Letters 23, 1207 (1969).
- 6 S.J. Silvers, T.H. Bergeman, and W. Klemperer; J. Chem. Phys. 52, 5385 (1970).
- 7 J.C. Pebay-Peyroula; Physics of the One-and Two-Electron Atoms (North Holland Publishing Co., Amsterdam, 1969) pp. 348-361.
- 8 J.W.S. Rayleigh; Proc. Roy. Soc. 102, 1900 (1922).
- 9 H.H. Stroke; Physics Today, Oct. 1966, pp. 55-60.
- 10 R.W. Wood and A. Elet; Proc. Roy. Soc. 103, 396 (1923).
- 11 W. Hanle Zeits. f. Physik 30, 93 (1924).
- 12 G. Breit; J. Opt. Soc. Amer. 10, 439 (1925).
- 13 A.C.G. Mitchell and M.W. Zemansky; loc.cit. pp. 258-318.
- 14 H.W.B. Skinner; Proc. Roy. Soc. A 112, 642 (1926).
- 15 M. Lombardi and J.C. Pebay-Peyroula; Compt. Rend. 261, 1485 (1965).
- 16 Jean-Pierre Descoubes; C.R. Acad. Sc. Paris 259, 327 (1964).

- 17 Patrick Cahill, Richard Schwartz, and A. Norman Jette; Phys. Rev. Letters 19, 283 (1967).
- 18 G.H. Dieke; J. Mol. Spetr. 2, 494 (1958).
- 19 P.A. Franken, Phys. Rev. 121, 508 (1961).
- 20 G.H. Breit; Revs. Modern Phys. 5, 91 (1933).
- 21 F.D. Colegrove, P.A. Franken, R.R. Lewis and R.H. Sands; Phys. Rev. Letters 3, 420 (1959).
- 22 M. Born and R. Oppenheimer; Ann. Physik 84, 457 (1927).
- 23 G. Herzberg; Spectra of Diatomic Molecules (D. Van Nostrand Company Inc. 1966) see especially pp. 218-226.
- 24 P.M. Davidson; Proc. Roy. Soc. A 138, 580 (1932).
W. Richardson; Molecular Hydrogen and Its Spectrum (Yale University Press, 1935).
- 25 Von I. Kovács and A. Budó; Hung. Acta Physica 1, 1 (1949).
- 26 P.G. Burke, H.M. Schey, K. Smith; Phys. Rev. 129, 1258 (1963)
A brief account of the state of low energy electron-atom scattering theory as of 1964 is given by E. Gerjuoy in Physics Today 18, 24 (May 1965).
- 27 L.D. Landau and E.M. Lifshitz; Quantum Mechanics, (Addison-Wesley Publishing Co. Inc. Reading Mass. 1958, second edition) §145. Although the authors give only inelastic collision cross-sections, following through their derivation, the matrix elements are easily found under the same conditions.
- 28 R.R. Bockemuehl, General Motors Research Laboratories, Warren, Michigan.
- 29 W. Happer and E.B. Saloman; Phys. Rev. 160, 29 (1967). The authors of this paper attribute the phase shift plates to A. Lurio, R. Garwin, and A. Patlach of I.B.M. Watson Laboratory, Columbia University, New York.
- 30 G.H. Dieke, S.P. Cunningham, and F.T. Byrne; Phys. Rev. 92, 81 (1953).
- 31 L.D. Landau and E.M. Lifshitz; loc.cit. §107.
- 32 J.H. Van Vleck; Phys. Rev. 33, 467 (1929).
- 33 J.K.L. MacDonald; Proc. Roy. Soc. A 138, 193 (1932).

- 34 I. Martison, W.S. Bickel, J. Bromander, H.G. Berry,
L. Lundin, R. Buchta, and I. Bergstrom; J.Opt. Soc.
Amer. 60, 352 (1970).
- 35 B. Descomps, J.C. Pebay-Peyroula and J. Brossel; Compt.
Rend. Acad Sci. 251, 941 (1961).
- 36 J.P. Descoubes; Physics of the One-and Two-Electron Atom
loc.cit. p. 341.
- 37 W.R. Pendleton and R.H. Hughes; Phys. Rev. 138 A, 683 (1965).
- 38 P.T. Kindleman and W.R. Bennet; Bull. Amer. Phys. Soc. 8,
87 (1963).
- 39 R.G. Fowler, T.M. Holzberlein, C.H. Jacobson and
S.J.B. Corrigan; Proc. Phys. Soc. (London) A84, 539 (1964).
- 40 K.A. Bridgett and T.A. King; Proc. Phys. Soc. (London)
A92, 75 (1967)
- 41 L. Allen, D.G.C. Jones, D.G. Schofield; J. Opt. Soc. Am.
59, 842 (1969).
- 42 W.L. Wiese, M.W. Smith and B.M. Glennon; Atomic Transition
Probabilities, Vol. 1 NSRDS-NBS4 (U.S. Govt. Printing
Office, Washington, D.C., 1966).
- 43 F.W. Dalby and J. van der Linde; Colloque Ampere XV,
North-Holland, Amsterdam, 1969.